The effect of boundary layer dynamics and chemistry on the diurnal evolution of ozone in the daytime convective boundary layer.

Master thesis report

Roy Laurijsse
Reg.no 900403-504-090

22-05-2014
Wageningen University

Master thesis MAQ-81339
39 ECTS
Supervisor Meteorology and Air Quality: prof Maarten Krol

Preface

This report is a result of my master thesis. I AM studying environmental science, with a major in atmospheric quality and chemistry. Since my bachelor in environmental science, I became very interested in air quality and chemistry in general. I soon discovered that air quality was more than only chemical reactions, it includes a complex system in which lots of meteorological processes are involved that influence the chemistry within our atmosphere. These processes are involved on many scales, ranging from a local scale to a global scale. In order to know more about this, I followed several courses about these meteorological processes. The courses Boundary Layer Processes, Meteorology and Climate and Atmospheric Modelling were very useful for me in particular.

Air pollution has always been a hot item and is often in the news, especially smog is a trending topic. Smog exists when we have high chemical concentrations and favourable weather conditions. To understand these processes behind smog better, large measurement campaigns are launched. One of them is the PEGASOS project in which both chemical and meteorological data are collected. Unique to this data set is that they used a Zeppelin platform that collected upper air measurements. Most of the time these large data sets are not thoroughly investigated and this raised my attention. Me and Maarten Krol found a case in San Pietro Capofiume (Italy) that contained interesting ozone measurements. These ozone measurements indicated a concentration decrease in the morning, which is rare. I decided to investigate this case and tried to model the diurnal ozone evolution with a mixed-layer model. In the first part of the thesis I tried to make a general characterization of the dynamics and chemistry and in the second part I investigated the morning ozone decrease.

In the first place I want to thank my supervisor Maarten Krol, who gave me very good advice and support to make this a better thesis. Secondly, I also want to thank Jordi Vilà-Guerau de Arellano for the many hours he spent to improve this thesis. He also taught me the very basics of boundary layer processes, which was very useful in this thesis. I also want to thank Laurens Ganzeveld, who gave me useable information and advice. Finally, I want to thank my family and girlfriend for their support throughout my study.

Roy Laurijsse,

21-5-2014

Summary

Tropospheric ozone (O_3) is a dangerous compound that can damage humans and ecosystems on both global and local scale. At local scale this implies that it is important to understand how O_3 concentrations are behaving throughout the day and what factors are influencing them.

In this MSc thesis we focus on a case in San Pietro Capofium (SPC) where morning measurements of O_3 were collected with a Zeppelin platform, during the PEGASOS campaign on 12 July 2012. This Zeppelin takes measurements of the profiles of O_3, NO, NO_2, temperature and moisture from the boundary layer (From 80m to 700m altitude). Besides these Zeppelin measurements also surface observations are available at SPC. In the first part of the research, we study and interpret these observations by reproducing the case using a mixed-layer model. The model describes the essential components of the convective boundary layer (CBL) evolution. Furthermore, the dynamics of the model are coupled to a chemical module in which the essential chemical reactions of the O3-NOx-CO-VOC system are represented. With the model a validated case is made that serves as a control case in the sensitivity analyses. In the second part of the research we focus on the morning transition. During the morning of 12 July, 2012, a decreasing O_3 concentration was observed. To investigate the possible reasons for this O_3 decline in the morning, a sensitivity analysis is presented, in which three case studies are compared with the control case: 1) a run with dynamical dry deposition of ozone on plants, 2) “titration” of ozone by enhanced NO emissions in the early morning, and 3) a lower initial boundary layer height. As an additional case study, three different types of initial vertical O_3 profiles are investigated: 1) with an O_3 lapse rate of zero in the free atmosphere, 2) with a fixed O_3 lapse rate and 3) a combination of both O_3 lapse rates.

Our findings show that dry deposition by plants has only a small effect on the diurnal evolution of O_3. The impact of the initial boundary layer height on the surface ozone concentrations was found to be important. When comparing the surface and upper air conditions, we found that the surface conditions have a larger impact on the morning O_3 concentrations, and that upper air conditions have more influence on the afternoon O_3 concentrations.

Table of Contents

1. Introduction

Tropospheric ozone is a gaseous compound that, at high concentrations near the surface, can damage human and ecosystem health. Besides damaging the environment, ozone is also an important greenhouse gas (Ainsworth, Yendrek, Sitch, Collins, & Emberson, 2012). This implies that it is important to know how ozone concentrations are behaving throughout the day and what factors are influencing them. This thesis is focussed on a case in San Pietro Capofiume (SPC) where morning measurements of ozone were collected with a zeppelin, during the PEGASOS campaign on 12 July 2012. SPC is located near Bologna in the northern part of Italy. This area is also known as the Po valley, which is one of Europe's most polluted areas. In the Po valley are Italy's largest industrial cities located and high traffic densities. Furthermore, the Po valley is an enclosed basin surrounded by mountain ranges and the sea. In the north by the Alps, in the south by the Apennines and the Adriatic sea in the east.
Interestingly, it was observed that in the morning ozone concentrations at the surface are first declining and after some hours increasing again. This is illustrated in figure (1) (Rohrer, 2012). As investigated in previous studies the increase in ozone concentration in the morning can be ascribed in the first place to the mixing with the residual layer above. In this residual layer, ozone from the previous day is stored and can contribute up to 70% of the total tropospheric ozone concentrations in the atmospheric boundary layer (ABL) (Neu, Künzle, & Wanner, 1994). When the ABL is fully developed, chemical production will start to dominate the tropospheric ozone concentrations in the ABL. However, as mentioned we observed first a decrease in the ozone concentrations. According to literature, ozone can be removed during the night by dry deposition, chemical reaction with nitrogen monoxide (NO) and reactions with Volatile Organic Compounds (VOCs) (Morris et al., 2010). In this thesis, we will investigate if we can determine the most likely reason of the observed ozone decrease. The main objective will be to investigate the relative roles of boundary layer dynamics and chemistry on the abundance of ozone in a diurnal cycle of the atmospheric boundary layer. To investigate this research topic we will present a modelling study in which we first make a strong validated case from which a sensitivity analyses will be done. In this sensitivity analyses the focus will be on the possible roles of dry deposition, NO emissions, Initial boundary layer height and the free tropospheric ozone lapse rate. In this thesis we will not investigate the effect of VOC's on the diurnal evolution of O_3. Summarizing, the research questions are:

1. Is the model able to make a general characterization of the dynamics and chemistry for the 12th of July 2012 in San Pietro Capofiume
2. What are the possible roles of dry deposition, NO emissions, initial boundary layer conditions and free tropospheric lapse rate on the diurnal evolution of ozone in the daytime convective boundary layer in the Po valley?

2.1 What are the most likely contributors to the ozone concentration decrease in the morning?

2.2 What are the dominant processes that influence the diurnal evolution of ozone?: surface or upper air processes?

In this thesis, we will first outline the background theory in chapter 2. Followed by the research strategy in chapter 3, in which the model and the case studies will be explained and in chapter 4 we will summarize and present my results. We will end with a discussion and conclusion.

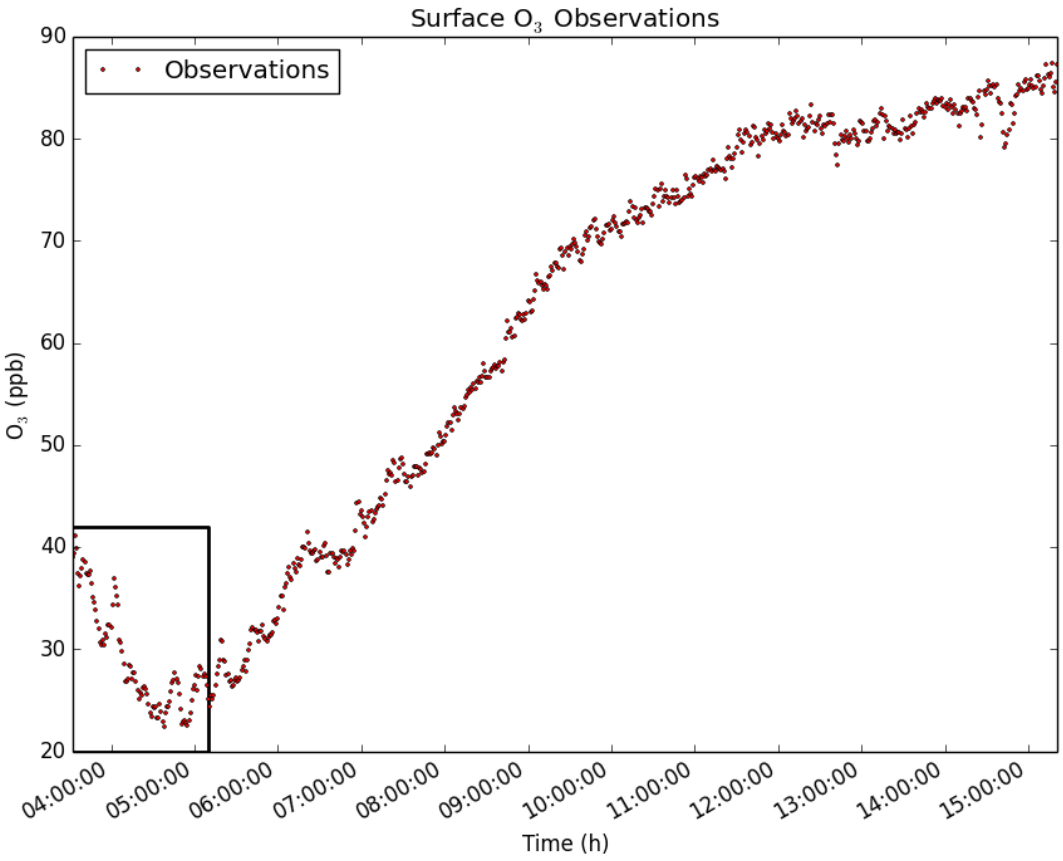

Figure 1:Diurnal evolution of Ozone (O3) measured at the surface near San Pietro Capofiume on the 12th of July 2012. The black square indicates the observed morning O3 decrease.

2. Theoretical background

2.1 Atmospheric boundary layer

The atmospheric boundary layer (ABL) is the lowest tropospheric layer and in direct contact with the surface. Therefore the ABL is directly influenced by the surface via heating from below and turbulence created by friction at the surface (Athanassiadis, Rao, Ku, & Clark, 2002). This ABL is a complex layer in which many chemical processes are taking place and can be described by several boundary layer dynamics. In the following chapters this will be explained in more detail.

During the day, the ABL changes rapidly. At sunrise, the ABL starts to grow due to heating from below. This heating from the surface causes the formation of thermal plumes. These thermal plumes will push the boundary layer to higher altitudes (Athanassiadis et al., 2002). On top of the ABL normally an inversion layer is located that is capping the ABL. This inversion is characterised by a temperature gradient and is often referred to as the entrainment zone (Conzemius & Fedorovich, 2006). When there are strong thermal plumes and strong turbulence near the top of the ABL, air from the free troposphere can entrain into the ABL. This air has another composition/chemistry than the air in the ABL and will affect its chemistry (Ganzeveld et al., 2008). After sunset, when heating from below stops and the turbulence decays, the ABL collapses and a nocturnal boundary layer (NBL) is created. This NBL is a stable layer and often only a few hundred meters thick. On top of this NBL a residual layer will remain. There is little mixing between the various layers. However, due to wind, turbulence can still occur and mixing between the layers can still happen (Morris et al., 2010). In figure (2) a representation of the evolution of the ABL is shown.

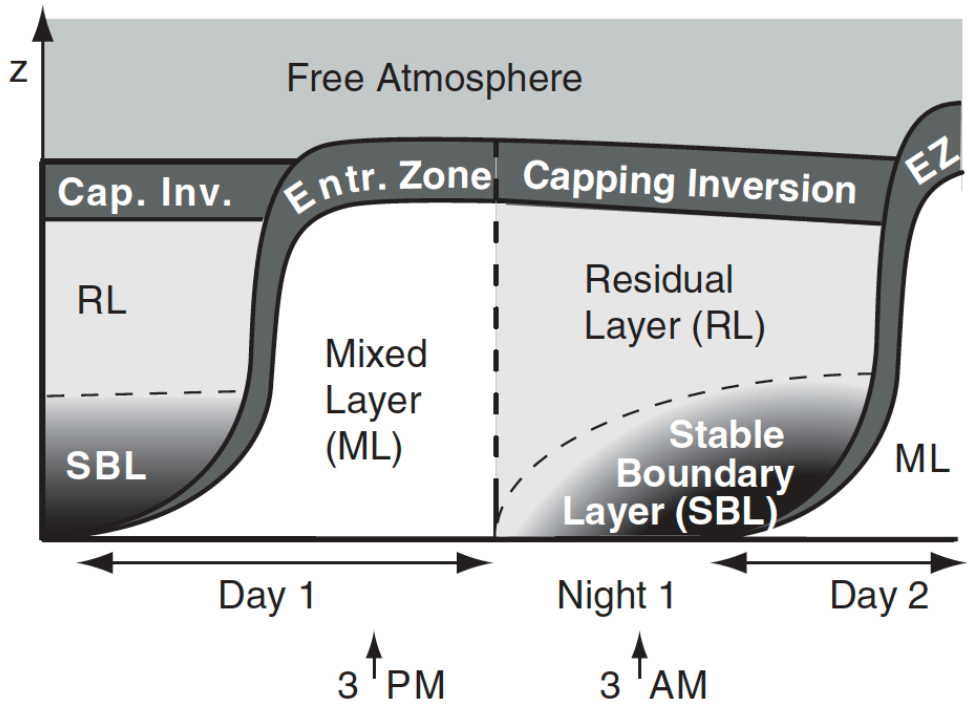

Figure 2: Diurnal evolution of an atmospheric boundary layer (Stull, 1988)

In the residual layer, chemical compounds from the previous day are stored. This happens when the ABL quickly collapses after sunset and the chemicals are trapped in the new residual layer (Morris et al., 2010). During the next morning when the ABL starts to grow, the ABL and residual layer will merge and mix again, implying that the chemicals that were trapped in the residual layer are reintroduced into the ABL. This leads to a change in the composition and chemistry of the ABL during that day (Zhang & Rao, 1999). This merging and mixing process is the strongest in the morning, when the ABL is growing fastest.

2.2 Dynamics

For the development of the boundary layer, dynamics are very important. They play a key role in the way the boundary layer evolves during the day. Dynamics also play a role in the way chemistry reacts in the ABL. For example, radiation directly influences the photochemical production of ozone. However, ozone itself does not directly affect the diurnal variability of the ABL dynamics. The indirect effect of ozone on the dynamics could be via plants. Ozone can affect the stomata, which can affect the evaporation and thus the dynamics. It is found that this process is more important over longer timescales (Super, 2013). Important dynamical variables that characterize the ABL are: the radiation budget, the latent and sensible heat fluxes, the potential temperature, water vapour mixing ratio and boundary layer growth. These dynamics are also important to validate the model used in this thesis as will be explained later (section 3.1.1).

2.3 Chemistry

In the ABL various complex chemical processes take place, with many different compounds. One of the most important compounds is tropospheric ozone. In this thesis the focus is therefore on ozone and the compounds related with ozone. Some important compounds that play a major role in ozone chemistry are: NO, NO_2, VOC's (e.g. Isoprene), CO, CH_4 and OH (Vilà Guerau de Arellano et al., 2011). In the first section (2.3.1) the basic ozone chemistry will be outlined and in the second section (2.3.2) the diurnal evolution of ozone will be explained.

2.3.1 Ozone chemistry

Tropospheric ozone is an important component when considering the air quality in the ABL. When ozone occurs in high concentrations it can be dangerous to humans and the environment (Jana, Sarkar, Saha, & Midya, 2012). Many chemical processes are influenced by the presence of ozone. Tropospheric ozone plays especially an important role in photochemical reactions (i.e. reactions driven by sunlight). Variation in these ozone concentrations influences the lifetime and distribution of other tropospheric chemicals such as NO, NO2 and OH, and thereby changing the tropospheric chemical equilibrium (Jana et al., 2012). Due to human (i.e. emissions of NO and VOCs) and natural activities (photo-chemical reactions) the tropospheric ozone concentrations are increasing. Tropospheric ozone should not be confused with stratospheric ozone. This latter ozone is beneficial since it protects humans and the environment against dangerous radiation from the sun. Stratospheric ozone is mainly produced by the addition of a ground state oxygen atom O(3p) with molecular

oxygen O_2. This O(3p) is in a ground-level triplet state and is highly reactive. To ensure that there is still energy conservation a third body M is introduced to complete the reaction (D. Jacob, 1999). The reaction is shown below:

$$O + O_2 + M \rightarrow O_3 + M. \qquad (R1)$$

To produce this O(3p) oxygen has to react with ultraviolet (UV) light:

$$O_2 + h\nu\ (\lambda = < 240\ nm) \rightarrow O(3p) + O(3P) \qquad (R2)$$

In this thesis the focus is on tropospheric ozone, since our investigation takes place in the troposphere. Tropospheric ozone is created in a different way than stratospheric ozone. There are two ways to increase the tropospheric ozone in the ABL. The first way is the transport of ozone from the stratosphere into the troposphere and the second options is the production of ozone within the troposphere, by the cycling of NOx. In this NOx cycling also hydrocarbons are involved, these hydrocarbons are emitted by anthropogenic or natural processes (e.g. industry, trees). Two important hydrocarbons for the production of tropospheric ozone are CO and CH_4. When these hydrocarbons are oxidized by OH, respectively HO_2 and CH_3O_2 are produced. With the help of these two products, NO_2 can be produced via R6 and R7. Finally the NO_2 will photolysed and O_3 is produced (R8). This is the most important reaction within O_3 chemistry. (D. Jacob, 1999):

$$HO_2 + NO \rightarrow OH + NO_2 \qquad (R6)$$

$$CH_3O_2 + NO \rightarrow CH_3O + NO_2 \qquad (R7)$$

$$\mathbf{NO_2 + h\nu \overset{O2}{\leftrightarrow} NO + O_3} \qquad \mathbf{(R8)}$$

Since O_3 is produced by the reaction of NO_2 with sunlight (left site R8) and at the same time destroyed by the reaction with NO (right site R8), we have an equilibrium better known as the photo stationary state. When assuming we only have NO, NO_2 and O_3 in the ABL the main reactions concerning the photo stationary state are (Parrish et al., 1986):

$$NO_2 + h\nu \overset{JNO2}{\rightarrow} NO + O \qquad (R9)$$
$$O + O_2 + M \rightarrow O_3 + M. \qquad (R10)$$
$$NO + O_3 \rightarrow NO_2 + O_2 \qquad (R11)$$

From these reactions we can deduct the equation for the photo stationary state as (Parrish et al., 1986):

$$\varphi = \frac{J_{NO2}[NO_2]}{k_{11}[NO][O_3]} \qquad (1.0)$$

In which J_{NO2} is the photo dissociation rate for NO_2 and k_{11} the reaction rate for reaction R11. When φ=1 both reactions are in equilibrium and there will be no production or destruction of O_3. However, when more complex chemistry is included this equilibrium can be shifted

and φ will change. When φ<1 we will have O_3 destruction and when φ>1 we will have O_3 formation. In reality this equilibrium is often disturbed, since we have a complex chemical system in which also other compounds are involved like OH, CO and VOC, shifting the equilibrium.

There are several ways to lose O_3 from the ABL. The first way to lose O_3 from the ABL is the reaction of an O(1d) atom with another compound e.g. H_2O. As a result, two OH radicals are formed and one ozone molecule is lost. Another way to lose ozone from the ABL is the direct reaction of O_3 with HO_2 and OH (R13 and R14). These reactions are only relevant in remote places of the troposphere where low NOx concentrations prevail (D. Jacob, 1999).

$$O(1D) + HO_2 \rightarrow 2OH \qquad \text{(R12)}$$

$$HO_2 + O_3 \rightarrow OH + 2\,O_2 \qquad \text{(R13)}$$

$$OH + O_3 \rightarrow HO_2 + O_2 \qquad \text{(R14)}$$

Many more mechanisms are involved in ozone chemistry. However, the above-mentioned reactions are the main reactions that drive ozone chemistry. In figure (4) the main ozone reactions are given. Notice that O_3 chemistry is more complex then explained above.

There are many more mechanisms involved in tropospheric O_3 chemistry. One of these mechanisms is O_3 production via volatile organic compounds (VOC's). VOC's can be natural emitted by trees (Isoprene) or anthropogenic by industry. As an example the mechanism with VOC's is shown below (Jana et al., 2012):

VOC + OH + O2 → RO2 +H2O
RO2 +NO+O2 → NO2 +HO2 + CARB (Secondary VOC)
HO2 +NO → NO2 +OH
2 (NO2 + *hv* +O2 → NO + O3)
Net: (NOx+OH)+ VOC+ 4O2 → 2O3 + CARB+H2O + (NOx+OH)

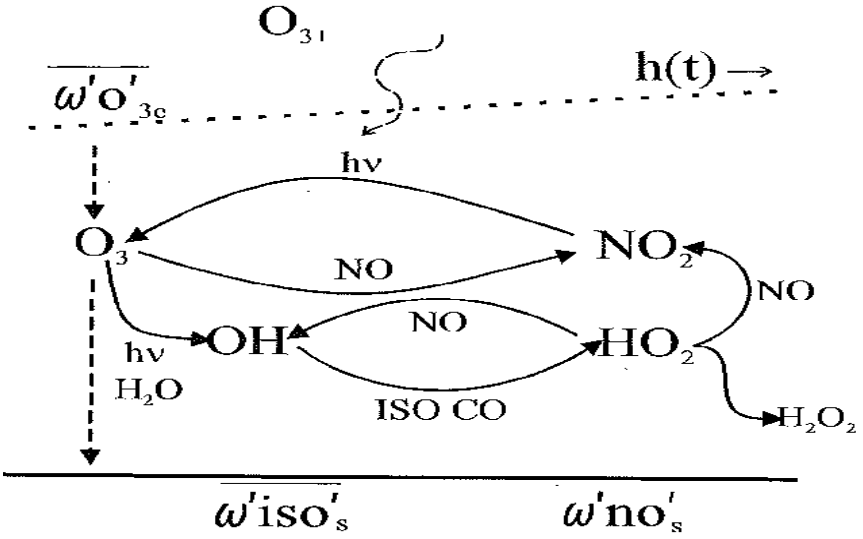

Figure 3: Main chemicals and dynamical processes that control the tropospheric ozone concentrations (D. Jacob, 1999)

2.3.2 Diurnal ozone evolution

During the day the ABL can normally be considered as a well-mixed layer and ozone is mixed across the whole ABL. The lifetime of ozone is determined as the time that ozone stays in the boundary layer. There are three main processes that determine the lifetime of tropospheric ozone in the boundary layer: 1) the reaction of ozone with hv light (O_3 + hv (H_2O)-> 2OH), 2) the reaction of ozone with OH or HO_2 (OH + O_3-> HO_2+ O_2 and HO_2 +O_3 -> OH + 2O_2) and 3) deposition of ozone towards the surface (D. Jacob, 1999). Due to these removal processes the chemical lifetime of ozone ranges from a week in the tropical lower troposphere to several months in the upper troposphere and extra tropical winter (D. J. Jacob, 2000). Other literature approximate the chemical lifetime to be around 22 days (Stevenson et al., 2006).
After sunset the heating from the ground ceases and the turbulence will decay (Morris et al., 2010). Therefore, the ABL collapses and ozone is trapped in the newly created residual layer aloft. In the NBL below ozone decreases due to deposition and NOx titration, as a result the ground-level ozone concentrations are decreasing (Morris et al., 2010; Zhang & Rao, 1999). In general there is little mixing between the NBL and residual layer, but when strong turbulence occurs during the night (e.g. caused by wind) some mixing between the layers can take place. This turbulence is typically caused by high wind speeds near the surface (Morris et al., 2010). When this occurs, surface level ozone concentrations will sharply increase. Once the boundary layer starts to grow again in the morning, ozone from the residual layer is mixed back into the ABL. This process can contribute up to 70% of the total ozone concentration in the ABL during that morning (Neu et al., 1994). Afterwards, when the chemical production of ozone and growth of the boundary layer starts to advance these will become the most dominant processes influencing ozone concentrations (Neu et al., 1994).

3. Methods

In this chapter, we will explain the methods used in this thesis. First, we will describe how the mixed layer model works and we will explain the mixed layer theory. Secondly, we will give a description of the observations, the location and weather characteristics at San Pietro Capofiume. Thirdly, we will explain how the dynamics and the chemistry in the model will be validated. Finally, we will explain the sensitivity analyses and the four associated case studies.

3.1 Model explanation

In order to reproduce the diurnal variability of the CBL a mixed boundary-layer model (MXLCH) is used. This model makes it possible to describe the essential components of the CBL evolution. The model makes use of a simple description of the main processes such as turbulent mixing and entrainment. Furthermore, the model is coupled to a chemical module in which the essential chemical reactions of the O3-NOx-CO-VOC system are represented (Vila, 2009). In figure (3) below, a schematic representation of the dynamics is presented that describes the evolution of the convective boundary. This figure also represents the mixed layer model used in this thesis. In this section we will first explain the mixed layer theory and afterwards how it is applied on the heat (3.1.2), moisture (3.1.3), momentum (3.1.4) and chemistry (3.1.5) budgets. Secondly, we will explain the energy balance and surface scheme (3.1.6). The equations and theory used in these sections are adopted from (vilà Guerau de Arellano & van Heerwaarden, 2013).

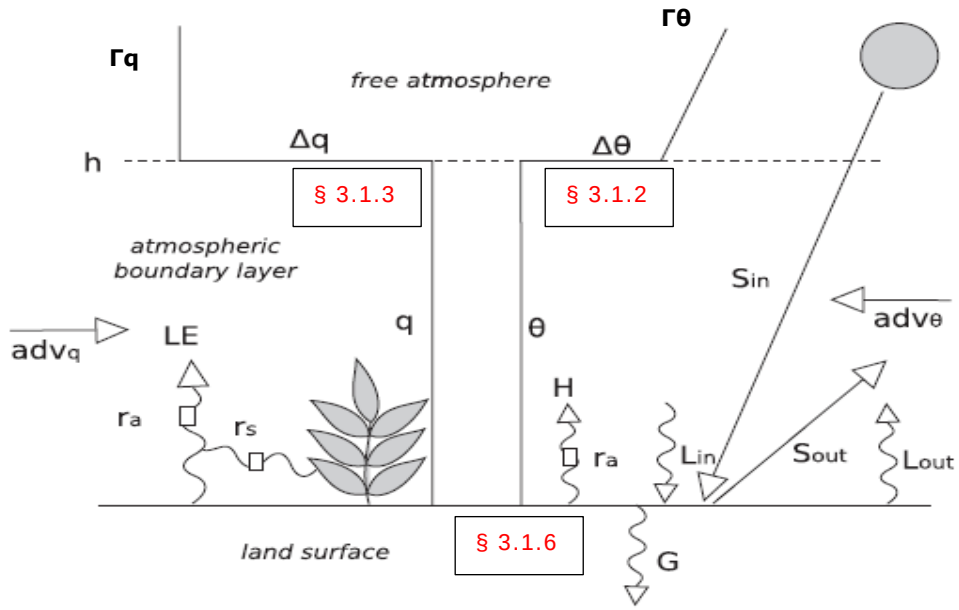

Figure 4: Schematic representation of the mixed layer model. The dynamics prescribing the boundary layer: Short and long wave radiation, latent (LE) and Sensible heat (H) fluxes, potential temperature (Θ), specific moisture (q) and boundary layer height (h) (Vilà Guerau de Arellano et al., 2011)

3.1.1 Mixed-layer theory

The model uses mixed-layer theory, which is visually presented in figure (3). As a basis for the mixed-layer theory, three basic equations are used. These equations are the result of vertical integrating the conservation equations for momentum, heat, moisture and chemical reactants. The general conservation equation reads:

$$\frac{\delta\varphi}{\delta t} + u_j \frac{\delta\varphi}{\delta x_j} = \begin{cases} F/m \\ S \end{cases} \qquad (1.0)$$

In the equation, the atmospheric quantities are represented by a generic variable (φ). These atmospheric quantities are mass (density, ρ), momentum (the three wind components u, v and w), heat (potential temperature, θ), water vapour (specific moisture, q) and chemical species (O_3, NO and NO_2). Furthermore, the first term on the left hand side is the temporal evolution of (φ) and the second term is the advection of (φ) by wind. On the right hand side F/m and S, represent the forces per unit of mass and sources/sinks averaged over the entire ABL. For example for a chemically active compound, where S represents the production/destruction by chemical reactions and for heat, S represents potential temperature changes by a radiative flux divergence. Before explaining the basic mixed layer equations, we need to make some important assumptions. We assume that the ABL flow is horizontally homogeneous for all variables. In mathematical terms this can be expressed as $\frac{\delta}{\delta x} = \frac{\delta}{\delta y} = 0$. Physically this means that, in these basic equations we temporary assume that there is no advection. Additionally, we assume that the mean vertical velocity (w) within the CBL is zero. Meaning, that we only take the vertical turbulent flux ($\overline{(w'\varphi')}$) into account. Finally, we make use of the fact that often all atmospheric quantities are well mixed in the CBL. As a result, the entire variation of the variable over the whole vertical domain is well represented by a single mixed layer value. It is also important to mention that the atmospheric quantities represented by φ remain constant with height and the vertical gradient of these quantities remain unchanged over time, also known as the "quasi steady-state" condition. When considering these assumptions the mixed layer equations are:

$$\frac{\delta<\varphi>}{\delta t} = \frac{\overline{(w'\varphi')_s} - \overline{(w'\varphi')_e}}{h} + \begin{cases} < F > /m \\ < s > \end{cases} \qquad (1.1)$$

$$\overline{(w'\varphi')_e} = -\Delta\varphi_h \left(\frac{\delta h}{\delta t} - w_s\right) = -\Delta\varphi_h w_e \qquad (1.2)$$

$$\frac{\delta\Delta\varphi_h}{\delta t} = \gamma\varphi \left(\frac{\delta h}{\delta t} - w_s\right) - \frac{\delta<\varphi>}{\delta t} \qquad (1.3)$$

Equation 1.1 shows that the temporal variations in the mixed layer <φ> are due to a turbulent flux at the surface $(w'\varphi')_s$ and at the top of the boundary layer $\overline{(w'\varphi')_e}$, with respect to the boundary layer growth (h), which has a dilution effect.
The entrainment flux $\overline{(w'\varphi')_e}$ at the top of the boundary layer is described by equation 1.2, in which the exchange flux is related to the discontinuity between the free troposphere and the boundary layer (the jump), and the exchange rate (w_e). Notice that the entrainment

velocity (w_e) is defined as $w_e = \frac{\delta h}{\delta t} - w_s$ meaning that the boundary layer growth is suppressed by subsidence w_s.
We need an extra expression to represent the variation in this so-called jump. This is provided by equation 1.3, in which the free tropospheric value is related to the free tropospheric lapse rate (γ) and the entrainment velocity (w_e).
With these equations, it is possible to describe the diurnal variation of the atmospheric quantities in the ABL. For most atmospheric quantities, we need to adjust these equations, by describing the forces and sources/sinks and rewrite the equations. In the following sections, we will explain the prognostic equations for heat, moisture, momentum and atmospheric chemistry in more detail.

3.1.2 Heat budget

The heat budget is represented by the potential temperature and plays an important role in the structure and evolution of the diurnal ABL. It plays a significant role in the main driving processes such as convective turbulence, which is dependent on the heat distribution and evolution within the ABL. In the previous section (3.2.1) the basic equations are given. For the heat budget, we substitute φ in the equations (1.0, 1.1, 1.2 and 1.3) into θ. When we assume a horizontally homogenous dry CBL, with no influence by radiation divergence and latent heat (S=0). Then the conservation equation for heat reads:

$$\frac{\delta \bar{\theta}}{\delta t} = \frac{\delta \overline{(w'\theta')}}{\delta z} \qquad (2.0)$$

When applying the mixed layer theory we will end up with the following equations. These equations will drive the heat budget in the diurnal ABL:

$$\frac{\delta <\theta>}{\delta t} = \frac{\overline{(w'\theta')_s} - \overline{(w'\theta')_e}}{h} \qquad (2.1)$$

$$\overline{(w'\theta')_e} = -\Delta\theta_h \left(\frac{\delta h}{\delta t} - w_s\right) \qquad (2.2)$$

$$\frac{\delta \Delta\theta_h}{\delta t} = \gamma\theta \left(\frac{\delta h}{\delta t} - w_s\right) - \frac{\delta <\theta>}{\delta t} \qquad (2.3)$$

Equation 2.2 can also be rewritten, and this newly rewritten equation describes the boundary layer growth during the day ($\frac{\delta h}{\delta t}$) as follows:

$$\frac{\delta h}{\delta t} = -\left(\frac{\delta \overline{(w'\theta')_e}}{\Delta\theta_h}\right) + w_s \qquad (2.4)$$

From equation (2.4), we see that the boundary layer grows due to the entrainment of warm air and is suppressed by subsidence (meaning that w_s is negative) in high-pressure situations. We still need to solve the entrainment flux. To solve this we assume an important closure for these set of equations, we relate the surface heat flux to the entrainment heat flux as:

$$\overline{(w'\theta')_e} = -\beta \overline{(w'\theta')_s} \qquad (2.5)$$

In which β is a constant and we assume that β is equal to 0.2. Meaning, that 20% of the heat contribution in the CBL is due to the entrainment of heat at the inversion layer. The entrainment flux also depends on the moisture flux and the shear in the atmospheric surface layer as will be explained in the following sections.

3.1.3 Moisture budget

Now we add the moisture budget to the heat budget, meaning that we are completing the thermodynamic variables. When combining the moisture budget with the heat budget, we need to introduce a new concept namely buoyancy. Buoyancy is an upward flux that plays a key role in the boundary layer development. This buoyancy flux can be defined as $\overline{(w'\theta_v')}$, in which θ_v is the virtual potential temperature. The virtual potential temperature is the potential temperature that dry air would need to attain to have the same density as moist air at the same pressure. Because we use the virtual potential temperature in the buoyancy flux, we can combine the potential temperature flux with the moisture flux. This is done in equation 3.0 in which we see both potential temperature and moisture as follows:

$$\overline{(w'\theta_v')} = < w'\theta' > +0.61(< \theta >< w'q' > + < q >< w'\theta' > + < w'\theta'q' >) \quad (3.0)$$

When substituting φ in the three mixed-layer equations (1.1, 1.2 and 1.3) by q we obtain the equations for the moisture budget:

$$\frac{\delta <q>}{\delta t} = \frac{\overline{(w'q')_s} - \overline{(w'q')_e}}{h} \quad (3.1)$$

$$\overline{(w'q')_e} = -\Delta q \left(\frac{\delta h}{\delta t} - w_s\right) \quad (3.2)$$

$$\frac{\delta \Delta q_h}{\delta t} = \gamma q \left(\frac{\delta h}{\delta t} - w_s\right) - \frac{\delta <q>}{\delta t} \quad (3.3)$$

In these equations above, we describe only the moisture budget. In order to combine the heat budget and the moisture budget we need to introduce the buoyancy flux into equation (3.2). Furthermore, we need to rewrite equation (3.2) to have an equation that can describe the boundary layer growth again as follows:

$$\frac{\delta h}{\delta t} = -\left(\frac{\delta \overline{(w'\theta_v')_e}}{\Delta \theta_{vh}}\right) + w_s \quad (3.4)$$

Where $\Delta\theta_{vh}$ is expressed in terms of θ and q as:

$$\Delta\theta_{vh} = \Delta\theta_h + 0.61(< q > \Delta\theta_h + < \theta > \Delta q_h + \Delta\theta_h \Delta q_h) \quad (3.5)$$

We have now combined the heat budget with the moisture budget. To close the equations we assume the same closure assumption as introduced in the heat budget, in which we related the surface flux with the entrainment flux given by equation (2.4).

3.1.4 Momentum budget

In this section, we introduce the momentum budget and complete the thermodynamics that drive the atmospheric boundary layer dynamics. We include the horizontal wind components U and V and we add the Coriolis and pressure forces to the mixed layer equations. These two forces are representing the acceleration of the atmospheric boundary layer flow. By substituting in the equations (1.1 and 1.3) φ by U and V and adding the coriolis and pressure forces we obtain the following equations:

$$\frac{\delta <U>}{\delta t} = \frac{\overline{(w'u')_s} - \overline{(w'u')_e}}{h} + f_c(V_g - V) \quad (4.1)$$

$$\frac{\delta <V>}{\delta t} = \frac{\overline{(w'v')_s} - \overline{(w'v')_e}}{h} + f_c(U_g - U) \quad (4.2)$$

$$\frac{\delta \Delta U_h}{\delta t} = \gamma u \left(\frac{\delta h}{\delta t} - w_s\right) - \frac{\delta <U>}{\delta t} \quad (4.3)$$

$$\frac{\delta \Delta V_h}{\delta t} = \gamma v \left(\frac{\delta h}{\delta t} - w_s\right) - \frac{\delta <V>}{\delta t} \quad (4.4)$$

Where V_g and U_g are the geostrophic wind components and V and U the coriolis force components multiplied by coriolis force parameter (f_c). From the previous sections we have seen that we had every time three mixed-layer equations. We are missing the equation that is describing the entrainment flux and the boundary layer growth. Before we can derive this third equation, we need to introduce shear, also called mechanical turbulence. It is different from the early mentioned convective turbulence that is caused by density differences. Mechanical turbulence is the variation of the wind with height. The influence of shear is largest at the surface and near the entrainment zone. To introduce shear in the mixed layer equations we need to do a complex derivation in which we need to use a dimensionless analyses of the turbulent kinetic energy equation. This derivation is explained in the paper of Pino, Vilà-Guerau de Arellano, and Duynkerke (2003). For now, we simply modify equation (3.4) from section 3.2.3 resulting in:

$$\frac{\delta h}{\delta t} = -\frac{1}{\Delta\theta_{vg}}\left(\overline{(w'\theta_v')_e} + 5u_*^3\left(\frac{\theta_v}{gh}\right)\right) + w_s \quad (4.5)$$

Where U_* is the friction velocity and g the gravity constant. Notice that when there are calm conditions and no shear is present we end up with equation 3.4 again.

3.1.5 Atmospheric chemistry budget

In the previous sections, we explained the dynamical system of the mixed-layer model. In this section we will explain how the chemical part of the mixed-layer model is working. We still make use of the mixed-layer theory and the related equations given in section (3.2.1). The main difference is that we have other sources and sinks for the chemical species (φ). In general these sources and sinks ($S\varphi$) are a combination of production and loss reactions. Therefore, the mixed-layer equations for a reactant in the boundary layer reads:

$$\frac{\delta <\varphi>}{\delta t} = \frac{\overline{(w'\varphi')_s} - \overline{(w'\varphi')_e}}{h} + < S\varphi > \quad (5.1)$$

$$\overline{(w'\varphi')}_e = -\Delta\varphi_h\left(\frac{\delta h}{\delta t} - w_s\right) = -\Delta\varphi_h w_e \quad (5.2)$$

$$\frac{\delta\Delta\varphi_h}{\delta t} = \gamma\varphi\left(\frac{\delta h}{\delta t} - w_s\right) - \frac{\delta<\varphi>}{\delta t} + < S\varphi >_{h+} \quad (5.3)$$

Where $< S\varphi >$ is a combination of first and second order production (5.4) and loss (5.5) reactions:

$$\alpha + \beta \overset{k}{\rightarrow} \varphi \quad (5.4)$$

$$\varphi \overset{j}{\rightarrow} \alpha + \beta \quad (5.5)$$

$$< S\varphi >= k < \alpha >< \beta > -j\varphi \quad (5.6)$$

Where j is a first order reaction rate that depends on ultraviolet radiation and the photo-dissociation properties of the compound and k is the second order reaction rate depending on the atmospheric temperature, pressure and the presence of other air molecules (e.g. O_2, N and H_2O). When applying the theory for O_3 and considering the reactions given in the reaction scheme in appendix (II) table(2) we get the following mixed-layer equations:

$$\frac{\delta<O_3>}{\delta t} = \frac{\overline{(w'O_3')_s} - \overline{(w'O_3')_e}}{h} + < SO_3 > \quad (5.7)$$

$$< SO_3 > = PO_3 - LO_3 \quad (5.8)$$

In which PO_3 is the ozone production term and LO_3 the ozone loss term. We see that in the production term we use reactions R3, R4 and R5 from the reaction scheme (appendix (II)) and for the loss term we use reactions R1, R22 and R23. These reactions deviate from what we explained in section 2.3.1. However, these reactions as depicted here are used in the mixed-layer model and are slightly different but both have the same principles.

$$PO_3 = (k_3[N_2] + k_4[O_2])[O(1d)] + k_5[NO_2] \quad (5.9)$$

$$LO_3 = k_1 + k_{22}[NO] + k_{23}[NO_2] \quad (5.10)$$

3.1.6 Energy balance and Surface scheme

We have seen the mixed layer equations for potential temperature, moisture, momentum and chemical species. In this section, we will explain the energy balance and the surface energy balance. Furthermore, the two land surface schemes will be explained.

In the model it is important to have the correct energy balance. The amount of energy is determined by the shortwave solar radiation and the longwave radiation that depends on clouds and soil properties. The equation to calculate the net radiation (Rn) at the surface is:

$$Rn = Sin + Sout + Lin + Lout \quad (6.1)$$

In which Sin and Sout represent the shortwave incoming and outgoing radiation. The longwave incoming and outgoing radiations are represented by, respectively Lin and Lout. In equation (6.1), the downward incoming fluxes are positive fluxes and the upward outgoing fluxes are negative fluxes. We need Rn to determine how much available energy we have for the sensible heat (source/sink in the heat budget) and latent heat flux (source/sink in the moisture budget). We call this the surface energy balance and can be expressed as:

$$Rn = H + LE + G \qquad (6.2)$$

Where H is the sensible heat (Wm^{-2}), L the latent heat (Wm^{-2}) and G is the heat flux into the soil (Wm^{-2}). Notice that the energy units are in Wm^{-2} while the units for the kinematic turbulent fluxes are in K/ms and g/kg/ms, for respectively the sensible and latent heat flux. To relate the kinematic turbulent heat and moisture flux to the dynamic fluxes H and LE, we need the following relation and conversion factor (Stull, 1988):

$H = \rho c_p \overline{(w'\theta')}_s$, the conversion factor is: $\rho c_p = 1231 \frac{w/m^2}{Kms^{-1}}$

$LE = \rho L_v \overline{(w'q')}_s$, the conversion factor is: $\rho L_v = 3013.5 \frac{w/m^2}{\left(\frac{kg_w}{kg_{air}}\right)ms^{-1}}$

For calculating, the partitioning of the available energy between the sensible and latent heat two surface schemes can be used. The first surface scheme is the Jarvis-Stewart scheme, which uses canopy conductance as a critical value to calculate the partitioning between the sensible and latent heat. The second surface scheme is the A-g_s scheme, in which the canopy conductance is calculated based on plant physiology. The advantage of A-g_s is that it is more physically based and fewer parameters are needed compared to the more standard approach of the Jarvis-Stewart model. (Schüttemeyer, Moene, Holtslag, & De Bruin, 2008). However, the A-g_s is more sensitive for dry conditions which result in larger uncertainties.

3.2 Observations

In June and July 2012 the PEGASOS campaign took place. During this campaign, a special Zeppelin platform was used to measure meteorological and chemical data at different heights in the boundary layer. During one flight, the zeppelin went several times up and down through the boundary layer, ranging from approximately 80 meters to 700 meters. The zeppelin measured different chemical compounds (e.g. O_3, NO and NO_2) and meteorological data (e.g. temperature and moisture). Beside the zeppelin, SPC also performs measurements at the surface, and monitors the moisture characteristics of the surface. There is a surface meteorological station, ground station, micro meteorological station, radio sondes station and an air quality station. In appendix (I) table (1) the variables measured at each measurement station can be found.

To be able to run the mixed-layer model, we need initial boundary layer and chemical conditions to guide the model. These initial conditions will be based on the measurements collected at the San Pietro Capofiume's (SPC) meteorological measurement site (44,6 North and 11.6 East). SPC is located in the North of Italy near Bologna. This region is also known as the PO valley, which is a large plain in a semi-closed basin. The Alps in the North, the Appennines in the Southeast and the Adriatic Sea in the East enclose the Po Valley. As a flatland basin shielded by mountains the area is characterized by calm winds, strong temperature inversions and fog (Bonafe, 2009).

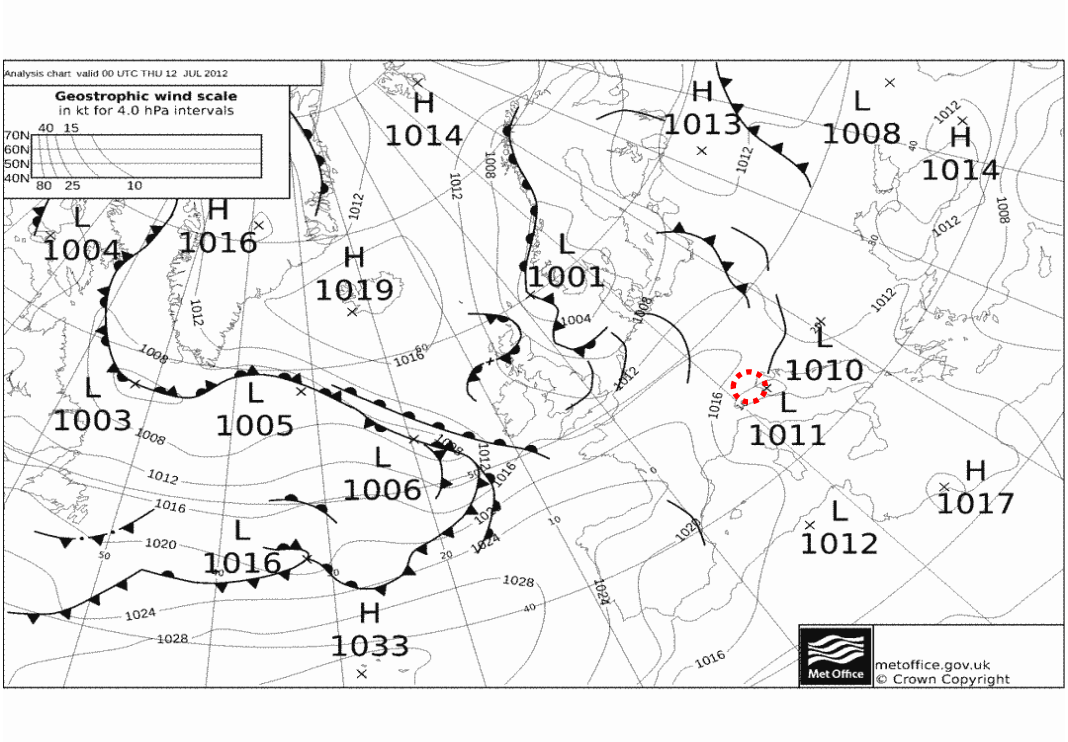

Figure 5: The synoptic situation for Europe, red dotted circle indicates the location of San Pietro Capofiume. (Adapted from Metoffice.gov.uk)

SPC's land cover is mainly grasslands, surrounded by crops. Furthermore, the SPC measurement site can be influenced by the nearby Sea and urban areas. In figure (5), the synoptic situation for Europe on the 12th of July is presented. SPC is located near the red dotted circle indicated in the figure. In figure (5), a typical thermal low above the Po Valley can be observed. This implies that the surface is heated quickly and that the less dense warm air can rise quickly (low subsidence). Consequently, the boundary layer height can grow to high altitudes (2300m) as can be seen in figure (6). Furthermore, low wind speeds and high temperatures on the 12th of July were recorded.

As mentioned above, the PEGASOS campaign took place in June and July 2012. There are two reasons to choose the 12th of July for this research. In the first place, on the 12th of July the zeppelin measured near SPC during the morning between 3:51 and 9:20 pm. Secondly,

the 12th of July is also a typical 'golden day', which means that there were no clouds during this day. There is one disadvantage on this day: Only one radio sonde released on the 12th at 11 AM. Since we are mainly interested in the morning transition, this radio sondes is not really useful. To solve this problem, we made a composite of the sondes released on the 11th and 12th of July. On the 11th of July four radio sondes were released, from which two in the morning (5:00 AM and 11:00 AM). To use these radio sondes, we made an average for the 11th and 12th of July for all observations. In this way we have a comprehensive data set that can be used for these two days.

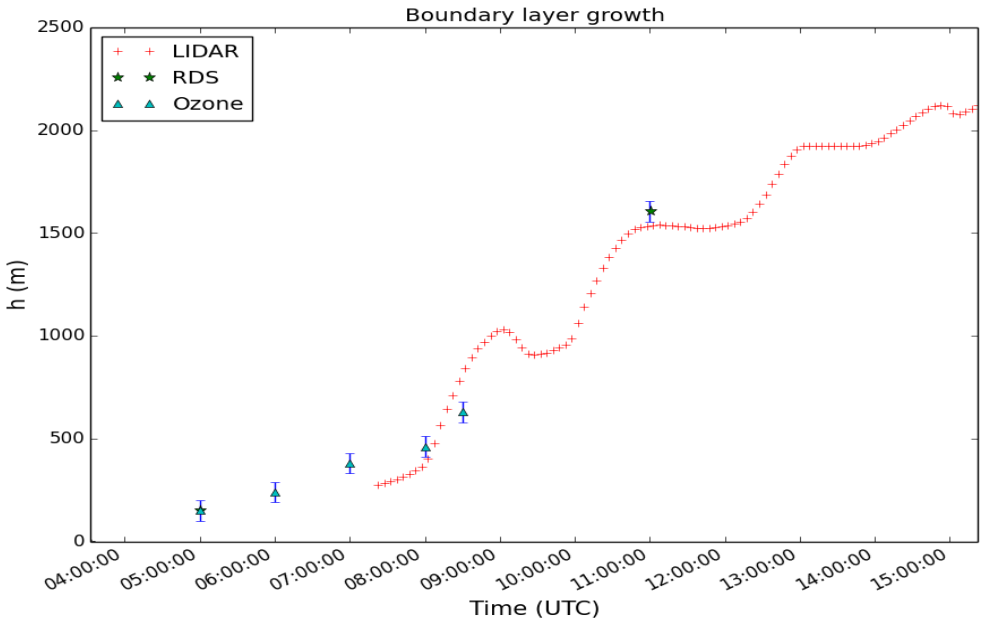

Figure 6: Boundary layer growth (up to 2300m). Measurements from LIDAR observations (red crosses), Radio sondes observations (green stars) and deducted from vertical ozone profile (cyan triangles)

3.3 Model validation and boundary conditions:

For the validation of the MXLCH model, we need to prescribe the initial and boundary conditions for the prognostic variables, surface fluxes, exchange fluxes and the free tropospheric conditions. These initial and boundary conditions are needed to calculate the surface fluxes and the temporal evolution of potential temperature, specific moisture, boundary layer growth and chemical species. An overview of the initial conditions for the dynamics and the chemistry are shown in appendix (III) tables (3),(4) and (5). Other important variables that we need are the location of the experiment (longitude and latitude), the day of the experiment, the running time of the model and the surface scheme. With the validation of the model, we mean that we want to reproduce the diurnal evolution as close as possible to the observations. These observations are collected during the PEGSASOS campaign at the San Pietro Capofiume measurement site.

We will first validate the dynamics and afterwards the chemistry. We first validate the dynamics since they determine to a large extent how the chemistry is behaving as we

explained in section (2.2). To validate the dynamics in a logical order, we constructed seven steps. In these seven steps, we will explain how to validate the dynamics for the MXLCH model see table (1). At the end this validated case will serve as my control case in the sensitivity analyses.

Table 1: Roadmap to validate the dynamics in the MXLCH model.

Step	
1	Location, day and surface scheme
2	Radiation energy balance
3	Surface energy balance
4	Potential temperature and specific moisture
5	Boundary layer height
6	Meso-scale
7	Vertical profile

3.3.1 Dynamics

As mentioned in the introduction of this section we validate the model in seven steps according table (1). The initial conditions and boundary conditions used can be found in table (3),(4) in appendix(III). The results of the control case will be shown in chapter 4.1.

The first step we need to do is to make sure that the model runs on the correct location, day and time. For the location, we use the longitude and latitude of the location (SPC) and for the correct day we use the day of the year (doy). We start the model at 3:30 AM and stop the model in the late afternoon at 3.30 pm. In this time, we capture the morning transition and the growth of the atmospheric boundary layer. To connect the surface with the atmosphere we have two surface-atmosphere schemes. As mentioned in section (3.1.1) we have the Jarvis-Stewart surface scheme and the A-gs surface scheme. In this research we have chosen for the Jarvis-Stewart scheme. The reason is that the A-gs surface scheme is not useable under very dry conditions. The problem with the A-g_s is when very dry conditions occur the surface resistance becomes too high, resulting in an error. In my case in San Pietro Capofiume, we have very dry conditions and when the A-g_s model is used the MXLCH model indeed gives an error.

Step 2 is to ensure that we have the correct radiation balance in the model. Based on the longitude, latitude and day of the year the model calculates the radiation components (Short and Long wave radiation). We improve the radiation balance by calculating the albedo from the observations by dividing the shortwave down radiation by the shortwave up radiation. As an extra option, we can mimic the aerosol effect by adding some cloud cover in the model. Because we have a golden day, we do not have to consider clouds in the model.

Step 3 is to validate the surface energy balance. We have two components in the surface energy balance that we need to validate, the first one is the sensible heat flux and the second one is the latent heat flux. In the previous chapter 2, we explained that heat flux is

very important for the boundary layer growth. To calculate the sensible heat flux we need to prescribe some initial conditions in the model. We need to prescribe initial conditions for: the potential temperature, the potential temperature jump, the free tropospheric potential temperature lapse rate, soil moisture and soil temperature. In order to calculate the latent heat flux we need to prescribe some different initial conditions: the initial mixed-layer specific moisture, initial specific moisture jump, free tropospheric specific moisture lapse rate, soil moisture and soil temperature.

Step 4 is to validate the potential temperature and specific moisture. These two quantities are already largely determined in the previous steps. In order to improve the calculation for both quantities, the initial conditions used in step three can be slightly adjusted. Something to keep in mind is that when the initial conditions are adjusted other dynamics can change as well. For example when adjusting the initial potential temperature this will have an effect on both the sensible heat flux and the potential temperature.

In step 5, we calculate the boundary layer growth. To do the calculation we need to prescribe the initial boundary layer height. From observations the initial boundary layer height is determined to be 150 meters (Rohrer, 2012). Notice that the boundary layer growth is also influenced by the initial conditions given in the other steps. In order to calculate the boundary layer growth, we need to consider these previous initial conditions. Vice versa, the boundary layer growth influences the evolution of the other dynamics (e.g. the latent and sensible heat, potential temperature and specific moisture).

In step 6, we include the large-scale processes to make the model more realistic. Possible large-scale processes that play a role are advection and subsidence. To justify the use of these processes we need weather charts to support our initial conditions. In figure (5) we see the synoptic situation of the 12th of July. From the figure we see that advection of heat is possible and that we do not have much subsidence, due to a thermal low.

In the final step 7, we have validated the important dynamics (Surfaces fluxes, temperature, moisture and boundary layer), based on their temporal evolution. For temperature and moisture we have also vertical profiles available. So to control the dynamics even more, these vertical profiles can be used to validate to model even better. From the model we can construct these vertical profiles by using the potential temperature and moisture content in the mixed layer, the jump at the top of the boundary layer and the free tropospheric lapse rate.

3.3.2 Chemistry

For the validation of the chemistry, we need to prescribe the initial conditions and boundary conditions for important chemical species. We are focussing on O_3 chemistry, meaning that the most important chemical species regulating O_3 chemistry are NO, NO_2 and VOC's. In section (2.3.1) the important reactions are already explained and an overview of the reactions used in the model are shown in appendix (II) table (2). The two most important compounds involved in O_3 chemistry are NO, and NO_2. VOC's are also important but we do not have sufficient measurements to constrain their concentrations as will be explained later.

For O_3, NO and NO_2 we need to prescribe the following initial and boundary conditions: (i) the Initial mixed-layer concentrations, (ii) the initial free troposphere concentrations and (iii) emission and/or (iv) deposition fluxes. Initially, these emission and deposition fluxes are assumed to be constant fluxes. In case of ozone, we also add some advection and we assume that there is no advection for other chemical species. In appendix (IV) table (3) the initial and boundary conditions for the important compounds can be found.
As mentioned before and explained in section 2.3.1 there are also other compounds involved bedsides O_3, NO and NO_2. For most of these compounds, we do not have sufficient measurements and therefore they cannot be validated. However, we are prescribing initial conditions for some of these compounds (ISO, CO and CH_4). There are measurements available for CO and CH_4, but due to their long presence in the atmosphere they do not play a significant role. In case of ISO we do not have sufficient measurements. However, ISO plays an important role in O_3 chemistry and therefore we estimate the initial conditions for ISO of 0 ppb (early morning) and an emission of 0.05 ppb/(m.s).

3.4 Sensitivity analyses

In the sensitivity analyses, we are first going to investigate the morning transition in which the nocturnal and residual layer merge into a convective boundary layer. As mentioned before, we have seen in the observations that ozone is decreasing in the early morning between 3:30 and 5 pm. There are several possibilities that can explain this morning O_3 drawback. We will investigate this O_3 decline in the morning by making three case studies that possibly explain the decrease of ozone in the morning period. These three case studies will be compared with the control case that is constructed in section (3.3). In the first case study, we will investigate the effect of dry deposition of O_3 and NO_2 on plants. In the second case study, we will investigate the effect of non-constant NO fluxes. Finally, in the third case study, we will investigate the effect of a lowered initial boundary layer height. Each case study continues on the previous case study. Beside these three case studies, we will do a fourth case study in which we will investigate the effect of different initial vertical O_3 profiles on the diurnal evolution of O_3 in the CBL. The reason for this extra case study is that we want to investigate the importance of upper-air conditions in comparison with surface conditions.

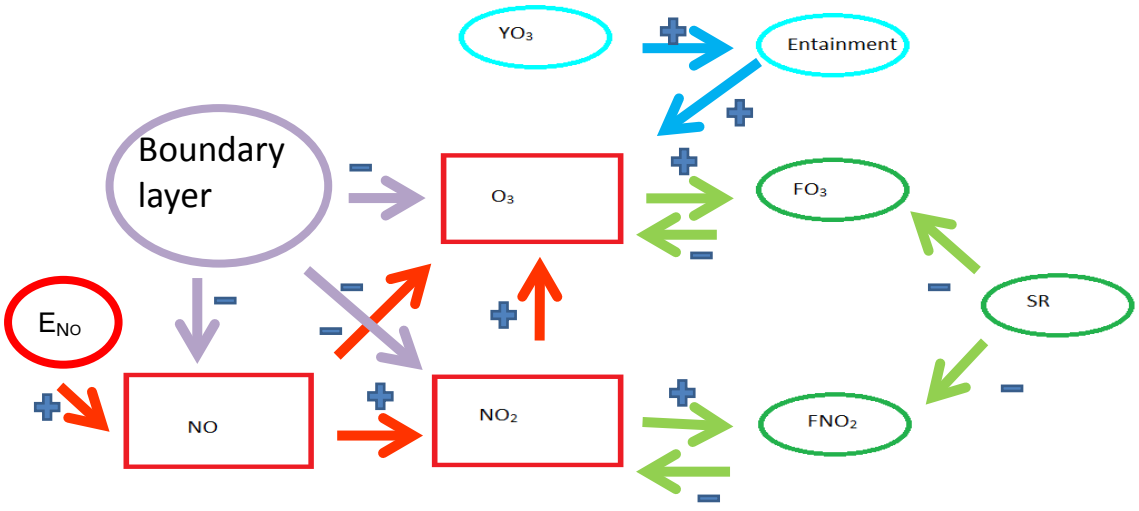

Figure 7: Conceptual diagram in which the four case studies are illustrated. Green represents case study 1, red case study 2, purple case study 3 and blue case study 4.

In the sections below, we will explain the control case and each case study in more detail. To have a clear overview of the case studies we made a conceptual diagram in which all the main processes and feedbacks are depicted (figure 7). In figure (7) in the green area, SR is the stomatal resistance and FO_3 and FNO_2 are the fluxes towards the plant better known as the deposition fluxes. The red area represents the atmospheric concentrations (ppb) for NO, NO_2 and O_3 and E_{NO} is the emission flux of NO (ppb m/s). In the purple area the effect of the boundary layer is illustrated and in the blue area YO_3 is the free tropospheric lapse rate.

Control case

Before we explain the set-up of the different case studies in more detail, it should be mentioned that all the case studies will be compared with the control case. This control case is constructed and explained in the previous sections (3.3.1 and 3.3.2). The control case is validated according the observations measured at SPC. In this control case we use constant emission and deposition velocities, a fixed free tropospheric lapse rate and an initial boundary layer height of 150 meter. Since the control case is adjusted such that a favourable comparison with the available measurements is obtained, the sensitivity simulations will generally show a deteriorated fit to these observations. However, the aim of the control simulations is to show the sensitivity of the system for perturbations and not to find the model settings that would lead to a better fit to the observations. The reason for this is the large amount of available "knobs" that can be tuned. Such an approach would require a more formal "inverse modelling" design. More information about the control case can be found in appendix (VI) in front of the case studies.

Case 1: Dry deposition of O_3 and NO_2 by plants

In this first case study, we will investigate the effect of dry deposition by plants on O_3 and NO_2. We will perform four experiments in this first case study: 1) no dry deposition for both O_3 and NO_2, 2) only dry deposition for O_3, 3) only dry deposition for NO_2 and 4) dry deposition for both O_3 and NO_2. The dry deposition flux used in these experiments will be calculated with an adapted Jarvis-Stewart surface scheme. In this adapted Jarvis-Stewart surface scheme, we added a dry deposition module that is able to calculate a dynamical dry deposition flux. Normally, the Jarvis-Stewart scheme does not calculate this dynamical deposition flux.

It is expected that when we use this dynamical dry deposition flux, the concentrations of both compounds will decrease, compared to the constant deposition flux used in the control case. However, since we are focussing on the early morning the impact of dry deposition on the atmospheric O_3 and NO_2 concentrations are expected to be low. The reason for this small impact is due to the very high stomatal resistance (closed stomata) in the morning. When the day advances, the stomata will open, and we will have a lower stomatal resistance and thus a higher dry deposition flux. In appendix (VI) table (7) more detailed information about the initial conditions for this case study can be found.

Case 2: Non-constant NO emissions

In the second case study, we will investigate the effect of non-constant NO emissions. This case study will continue on the previous case study. From literature (Morris et al., 2010) it is known that during the night NO reacts with O_3 to produce NO_2, as a result O_3 concentrations will decrease in the NBL. In this case the photo-stationary state equilibrium will not be in balance ($\varphi < 1$), since there is no light reaction R9 does not proceed, and O_3 will be removed from the atmosphere. We expect that when we increase the NO emissions the O_3 concentrations will decrease.

To investigate this theory we will run four experiments. In these four experiments we will change the amount of NO emitted and the time when NO is emitted. In figure (8) the basic set-up of the experiments can be seen. We will have the control case in which we use constant NO emission fluxes (Black line) and the experiment in which we will boost the emissions (Blue line) for 1.5 hour during the morning. The reason to change the intensity and time of when NO is emitted is to mimic traffic during rush hour or to see the effect of industry and fertilized agricultural lands (Bouwman, Boumans, & Batjes, 2002). From these sources it is known that they emit NO into the atmosphere. In appendix (VI) table (8) more information on the amount and times when the NO is emitted can be found.

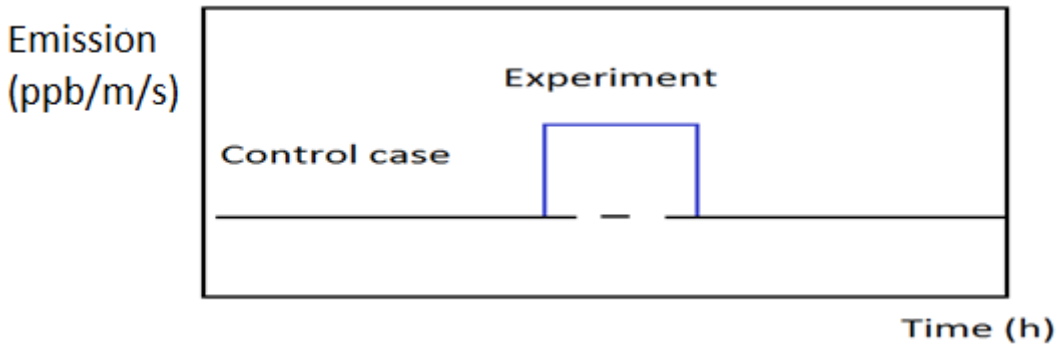

Figure 8: Set-up of the experiment. In the experiments, the NO emissions will be boosted for a short period (1.5 hours). More details can be found in appendix (VI) table 8

Case 3: Boundary layer height

In addition to the dry deposition and NO emission case studies, we will investigate the effect of a shallower boundary layer in the morning. It is expected that when we have a shallower boundary layer the concentrations of all chemical compounds will change. Due to this shallower boundary layer, we will have higher NO concentrations and lower O_3 concentrations, as explained in the previous case study.

Furthermore, in this case study, we will also combine three cases to see the total effect on the morning O_3 concentrations. We will increase the initial O_3 concentration to 40 ppb, so that we have a better comparison with the observations. Notice that when the initial boundary layer is changed other dynamics will change as well. Especially, potential temperature is expected to change. In figure (9) the growth of the boundary layer is depicted for the control case (Blue) and for the experiments (Cyan). We see that lowering the initial boundary layer height has only a small effect at the end of the day and the boundary layer starts to grow earlier in the morning. When we have a smaller boundary

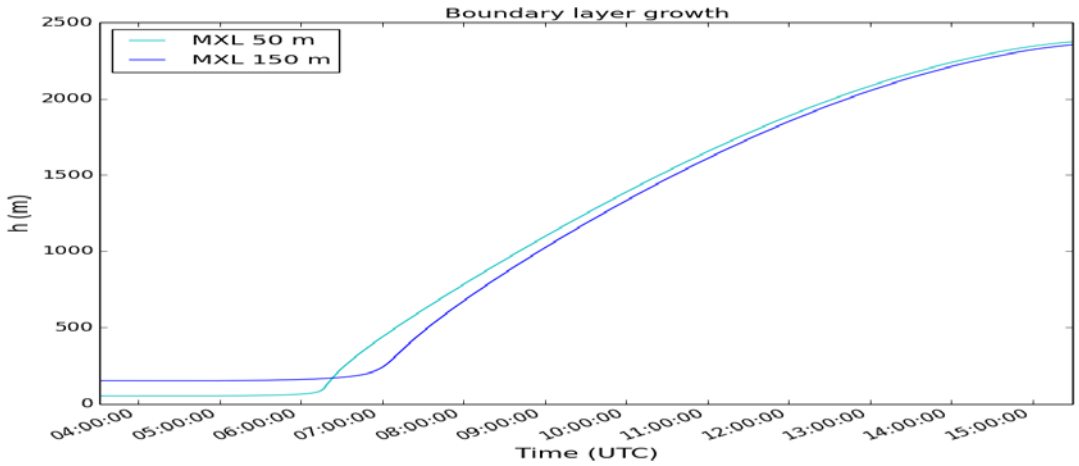

Figure 9: Boundary layer growth for the control case (blue) and the experiment (cyan).

layer less heat is needed to warm up the boundary layer and will grow earlier. In appendix (VI) table (9) the more detailed specifications for this case study can be found.

Case 4:Free tropospheric ozone Lapse rate

In this case study the importance of upper air conditions compared to surface conditions is investigated. We will compare three different types of vertical O_3 profiles, which are illustrated in figure (10). In the first vertical O_3 profile, we have a free tropospheric O_3 lapse rate of zero (ppb/m). In the second vertical O_3 profile, we have a fixed free tropospheric O_3 lapse rate of 0.0098 (ppb/m). These lapse rates are based on the observations made by the Zeppelin platform (appendix (V) figure (19)). Finally, in the third profile we will make a combination from the first two O_3 profiles. In this O_3 profile we will start with a lapse rate of 0.0098 (ppb/m) and we will end with a lapse rate of zero (ppb/m). Moreover, this combination is also based on what is observed by the Zeppelin. From the Zeppelin observations, we can distinguish three phases. In the first phase between 7 and 8 o'clock we have a lapse rate of 0.0098 ppb/m. The second phase is the transition phase in which the lapse rate starts to shift towards zero (ppb/m) and in the final phase around 9 o'clock the lapse rate is zero (ppb/m). This is mainly because the zeppelin is measuring in the CBL, in which we have a well-mixed layer. The height at which the lapse rate turns to zero takes is not exactly known. Therefore, in this thesis this height is assumed to be at 700m.

It is expected that when we have a larger lapse rate more O_3 can entrain into the CBL and

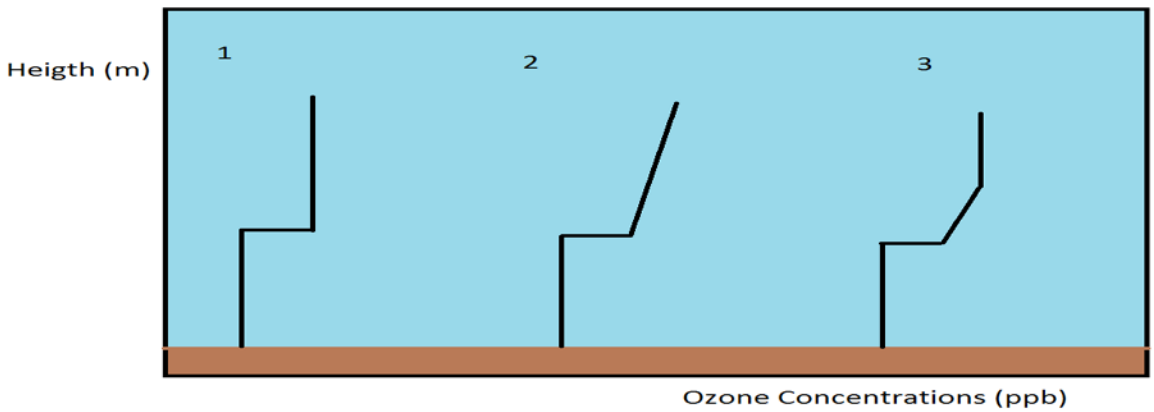

Figure 10: The three different vertical structure. Respectively from left to right: 1) No tropospheric lapse rate, 2) fixed tropospheric lapse rate and 3) combination of both structures

the concentrations will increase. Furthermore, we will compare case study 4 with the other three case studies, too see which case study has the largest effect on the diurnal evolution of O_3. In appendix (VI) table (10) more detailed information about this case study can be found.

4. Results

In this chapter an overview of the results will be given. First, we will present the results of the control case for both the dynamics and the chemistry. Secondly, we will present the results for the first three case studies of the sensitivity analyses. In which we investigated the morning O_3 decrease. Finally, we will present the results for case study 4 in which we compare the surface conditions with the upper air conditions.

4.1 Representation control case

4.1.1 Dynamics

In figure (11) we present the results for the dynamics. We see that in general the model is able to reproduce the dynamics very well compared to the observations. Especially the radiation balance matches very well with the observations. When we have a closer look to the other dynamics we see some differences between the model and the observations.

For both the sensible and latent heat flux we see that the model is overestimating compared to the observations. However, from literature we know that the observed latent and sensible heat fluxes can be slightly underestimated by approximately 11%. According to (Burns, Horst, Jacobsen, Blanken, & Monson, 2012) the main reason is that the measurement devices underestimate the vertical velocity. Consequently, the measured sensible and latent heat fluxes are underestimated. When considering these underestimations, the model results will be closer to the observations for both the latent and sensible heat flux.

The modelled potential temperature is in general lower than the surface observations, but higher than the radio sonde observations. Meaning, that the truth is somewhere in-between the surface observations and the radio sondes. For specific moisture we see that the model is consequently dryer than the observations. However, the trend is captured very well. We also observe the effect of dry air entrainment around 7:00 AM UTC in both the model and observations.

The boundary layer growth is slightly overestimated by the model compared to the observations. We see that the boundary layer starts to grow around 7:00 AM UTC, at the same time the entrainment of dry air started. Furthermore, we see that the model, radio sonde and LIDAR observations are matching quite well around 11:00 AM UTC.

In appendix (III) the vertical profiles for potential temperature and specific moisture are presented. We see that the model is not able to represent both vertical profiles correct compared to the observations. For the potential temperature we see that the vertical profile of the model is to warm and the same for moisture. We also see that the free troposphere moisture lapse rate is not in agreement with the observations. However, we had to find a compromise and this is considered to be the best fit to various observations.

Remember that we have a lot of opportunities to tune the model, meaning that when we have a good match or not this not mean that it is right or wrong. Most variables are interconnected with each other, when changing one parameter everything can change. We can improve the modelled vertical profiles for moisture and temperature. However, when

we do that, the temporal evolutions for moisture and temperature will change as well. For now, we are quite satisfied with the results, and use them as a starting point for sensitivity experiments.

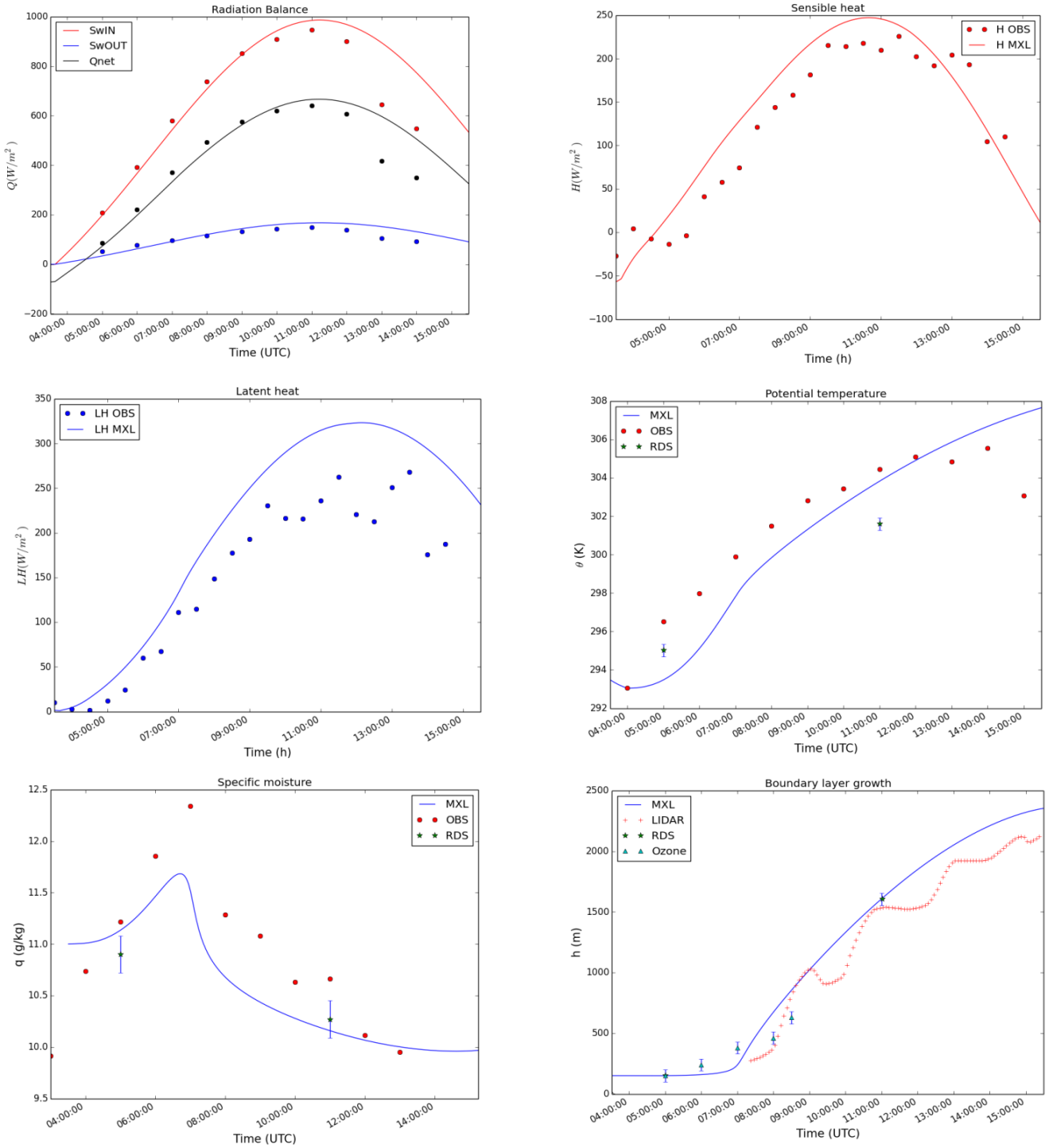

Figure 11: Temporal Evolution of the ABL dynamics observed and modelled respectively from top left to bottom right: Radiation Balance, Sensible heat flux, Latent heat flux, potential temperature, specific moisture, Boundary layer growth. In all plots the solid lines represent the model output (MXL), the observations (OBS) are represent by the dots. Some plots are supported with radio sondes (RDS), represented by the green stars. In the boundary layer growth plot the cyan triangles represent the boundary layer height according a vertical ozone profile (Ozone) and the red crosses represent the boundary layer height measured with LIDAR.

4.1.2 Chemistry

We continue with results for the chemistry, which are presented in figure (12). In this figure the temporal evolution of O_3, NO and NO_2 is presented. We see that the model is in general able to reproduce the diurnal evolution for all three compounds. However, for O_3 we see that the model is not able to capture the morning O_3 decrease and we see that the model is overestimating the concentrations between 7:00 AM and 9:00 AM UTC. This morning O_3 decline will be further analysed and investigated in the first three case studies.

An explanation for the overestimation between 7:00 AM and 9:00 AM UTC could be the entrainment of O_3 rich air from aloft. From the Zeppelin observations and the vertical profiles calculated by the model (appendix (IV) figure (19)), we see that we have higher O_3 concentrations in the free troposphere (65 ppb) than in the CBL (<65 ppb). When the CBL starts to grow this O_3 rich air from aloft is entraining into the CBL. This partly explains why there is rapid O_3 increase in the morning. Besides the entrainment, also the chemical production of O_3 starts to develop leading to even more O_3 in the CBL. This increase is observed both in the observations and in the model. However, the entrainment and chemical production are larger in the model, leading to a faster growth in the morning.

After 9:00 AM UTC we see that chemical O_3 production starts to dominate the entrainment of O_3 rich air. From the Zeppelin data we know that the free tropospheric O_3 concentrations are approximately 65 ppb. After 9:00 AM UTC the O_3 concentrations become larger than 65 ppb, meaning that there is another O_3 production source. We see that the O_3 concentrations grow until approximately 88 ppb, which is probably due to chemical production. To know how much chemical production or entrainment we have, an O_3 budget can be made. This O_3 budget can give an overview from all sources and sinks for O_3. In this thesis we did not managed to construct the O_3 budget.

In the graphs with NO and NO_2 we see that after 7:00 AM when the boundary layer starts to grow the concentrations are dropping rapidly and in the afternoon we see that the observed concentrations for both compounds are approximately zero. However, the modelled concentrations of both compounds do not reach zero. This is probably caused by the constant emissions that we apply in the model.

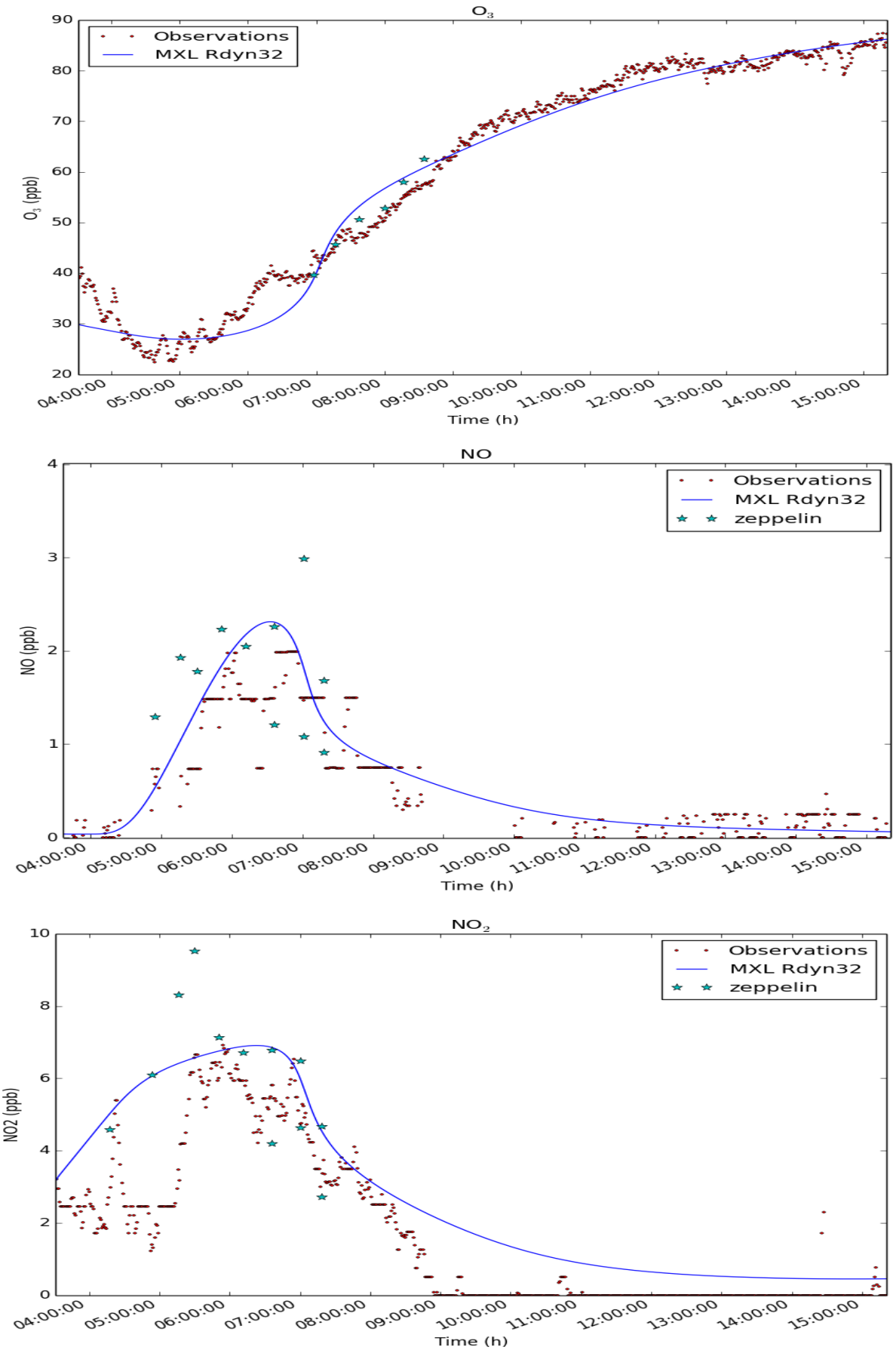

Figure 12: Diurnal evolution of ozone (O3), Nitric oxide (NO) and Nitrogen dioxide (NO2). Blue lines represent the model outcome, red dot represent the observations and the cyan stars are measured by the Zeppelin.

4.2 The morning ozone decrease

In this section, the results of the first three case studies will be presented. In which we investigated the morning O_3 decrease .

Case 1: Dry deposition of O_3 and NO_2 by plants

In figure (13), we can observe that dry deposition by plants has almost no effect on the O_3 decrease in the morning. Only at the end of the day, we see a small decrease in the O_3 concentrations. This effect is what we expected, because in the morning the stomata of the plants are still closed, resulting in a high stomatal resistance and a low deposition flux. Later on the day when the stomata are opened, the stomatal resistance decreases and the deposition flux increases. As a result, O_3 can enter the plant and O_3 concentrations will decrease in the CBL (Green line).

There is no interaction when we have a deposition flux for both O_3 and NO_2. We clearly see that O_3 concentrations are only decreasing when we have a deposition flux for O_3 (magenta line). We expected that when NO_2 concentrations are decreasing, less O_3 will be produced and will decrease (R9 and R10). Moreover, the NO concentrations are also decreasing, resulting in higher O_3 concentrations. Therefore, the removal and production for O_3 are in equilibrium and nothing happens with the O_3 concentrations (Photo-stationary state).

Both NO and NO_2 are mainly decreasing in the morning. This contradicts the theory mentioned before that the stomata are closed in the morning and no deposition can occur. This is something I do not understand and requires further analysis. Again we see that the deposition of O_3 alone has no noticeable effect on the NO and NO_2 concentrations.

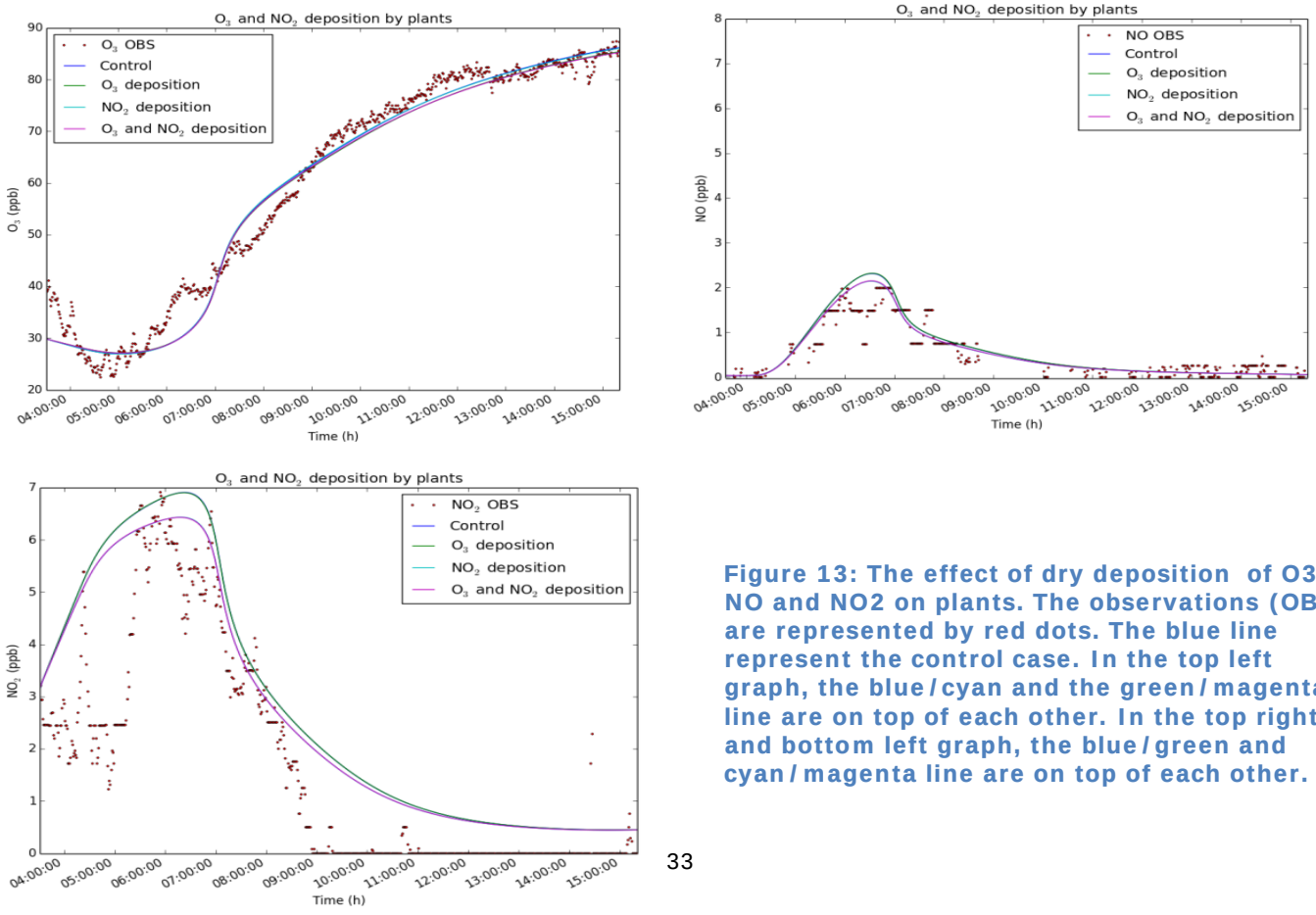

Figure 13: The effect of dry deposition of O3, NO and NO2 on plants. The observations (OBS) are represented by red dots. The blue line represent the control case. In the top left graph, the blue / cyan and the green / magenta line are on top of each other. In the top right and bottom left graph, the blue / green and cyan / magenta line are on top of each other.

Case 2: Non-constant NO emissions

When we include extra NO emissions in the morning, we see that the O_3 concentrations are decreasing (figure (14)). This decrease depends on the amount of NO emissions and the time of release. We see that when NO is emitted in the early morning with a four times higher emission rate, that the morning O_3 concentrations are decreasing the most (Cyan line). When we emit the same amount of NO later, we see that the O_3 decrease is smaller (Magenta line). When NO is emitted even later, we have an even smaller O_3 decrease (Yellow line). This large decrease in the morning is mainly because we have a shallow boundary layer with highly concentrated NO. When the boundary layer starts to evolve the NO concentrations are decreasing, due to a larger volume of the boundary layer and the entrainment of clean air from a loft. Therefore, we have less NO to remove O_3 and more O_3 is entering the CBL via entrainment and chemical production.

In figure (10) we have seen that when NO emissions are increased in the morning, that the NO concentrations are also increasing strongly. When these NO emissions are emitted on a later time the effect is decreasing. In general, we see that the NO emissions lead to a significant overestimate of the observations. After 12 AM we see that the NO concentrations become approximately zero, meaning that the volume of the CBL is large enough to reduce the NO concentrations to a minimum.

For NO_2 we see that the effect is approximately the same as for NO (figure (10)). We see an increase when the NO emissions are emitted and this effect is decreasing in. However, there are some clear differences. In the first place, we see a sharp turning point when the NO emissions are emitted and stopped. Secondly, we see a stronger increase in the NO_2 concentrations, than we see in the NO concentrations. This strong increase is mainly noticed in the morning, when NO removes O3 and NO_2 is produced.

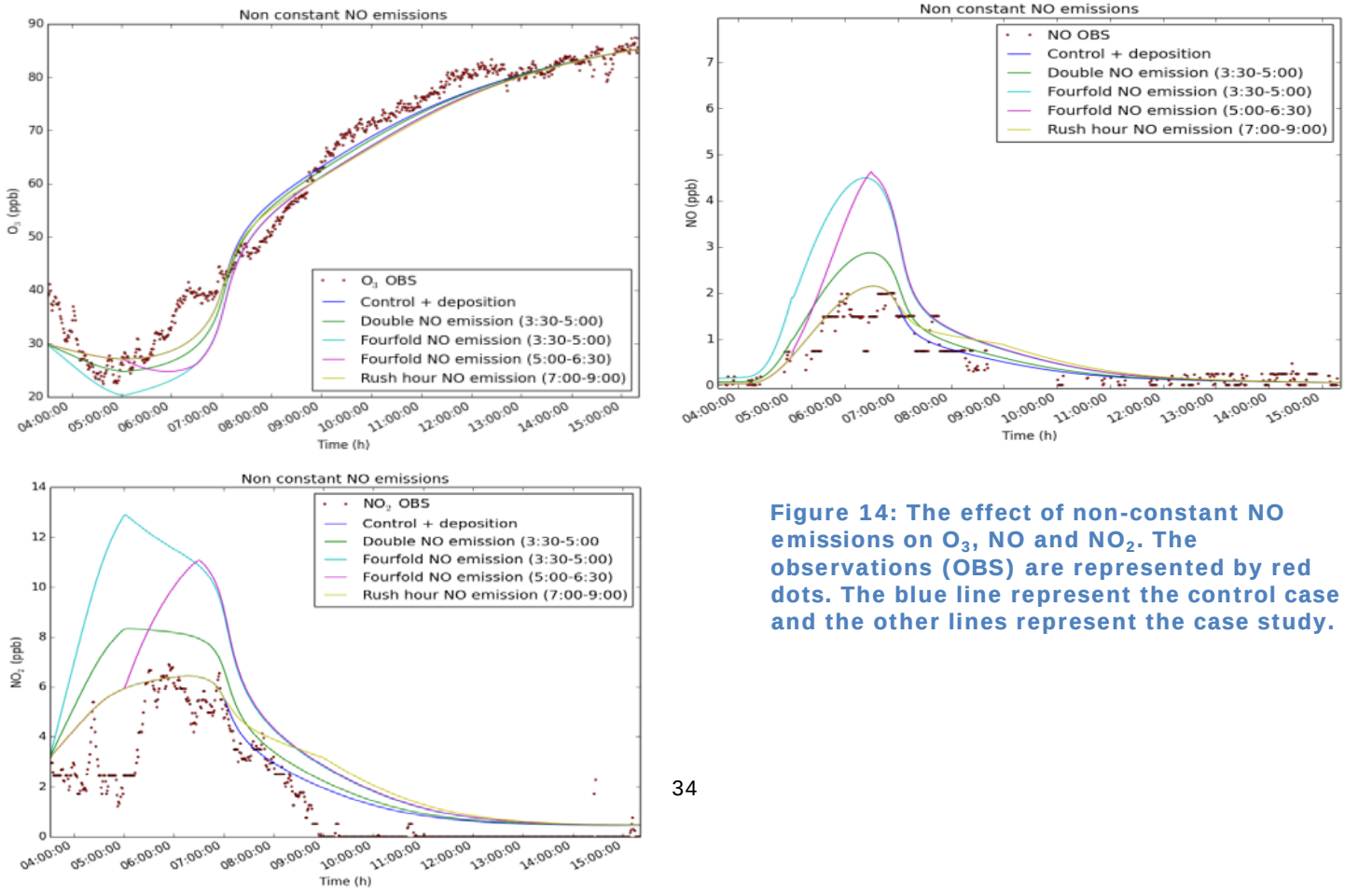

Figure 14: The effect of non-constant NO emissions on O_3, NO and NO_2. The observations (OBS) are represented by red dots. The blue line represent the control case and the other lines represent the case study.

Case 3: Boundary layer

In this case study, we changed the initial boundary layer height and increased the initial O_3 mixed layer concentration. Furthermore, we combined in this case study the other two case studies. In figure (15) we see the results of this case study for O_3, NO and NO_2. First we see that when the initial O_3 concentrations are increased from 30 ppb to 40 ppb, that NO_2 is also increased and NO is decreased (Green line). These increasing and deceasing concentrations are mainly in the morning and are due to the higher O_3 concentrations, which react with NO to produce NO_2. Secondly, when we lower the initial boundary layer height from 150m to 50m, we see that the O_3 concentrations are decreasing rapidly in the morning. While NO and NO_2 are increasing rapidly (Cyan line). The shallower boundary layer is the main reason why O_3 is decreasing fast, as we explained earlier. At the same time NO_2 is increasing due to the extra production, as a result of (R11). When the sun rises, the abundant NO_2 photo-dissociates and O_3 is rapidly produced (R9 and R10) and after 7:00 AM UTC, entrainment starts and O_3 rich air from aloft starts to entrain. Furthermore we see that the increase of O_3 and the decrease of NO and NO_2, starts earlier when we have a lowered initial boundary layer height. This shallower boundary layer is heated faster and as a result the inversion layer is broken earlier and the boundary layer starts to grow. Finally, when we combine the three case studies (Yellow line), we see that O_3 is decreasing even more and NO and NO_2 are increasing dramatically. However, when we consider the fact that we estimated the emission fluxes for NO and NO_2 and the possibility to tune the model, these results are not wrong. The objective of these case studies was to see the sensitivity of the diurnal O_3 evolution on certain perturbations and not to have a perfect fit with the observations.

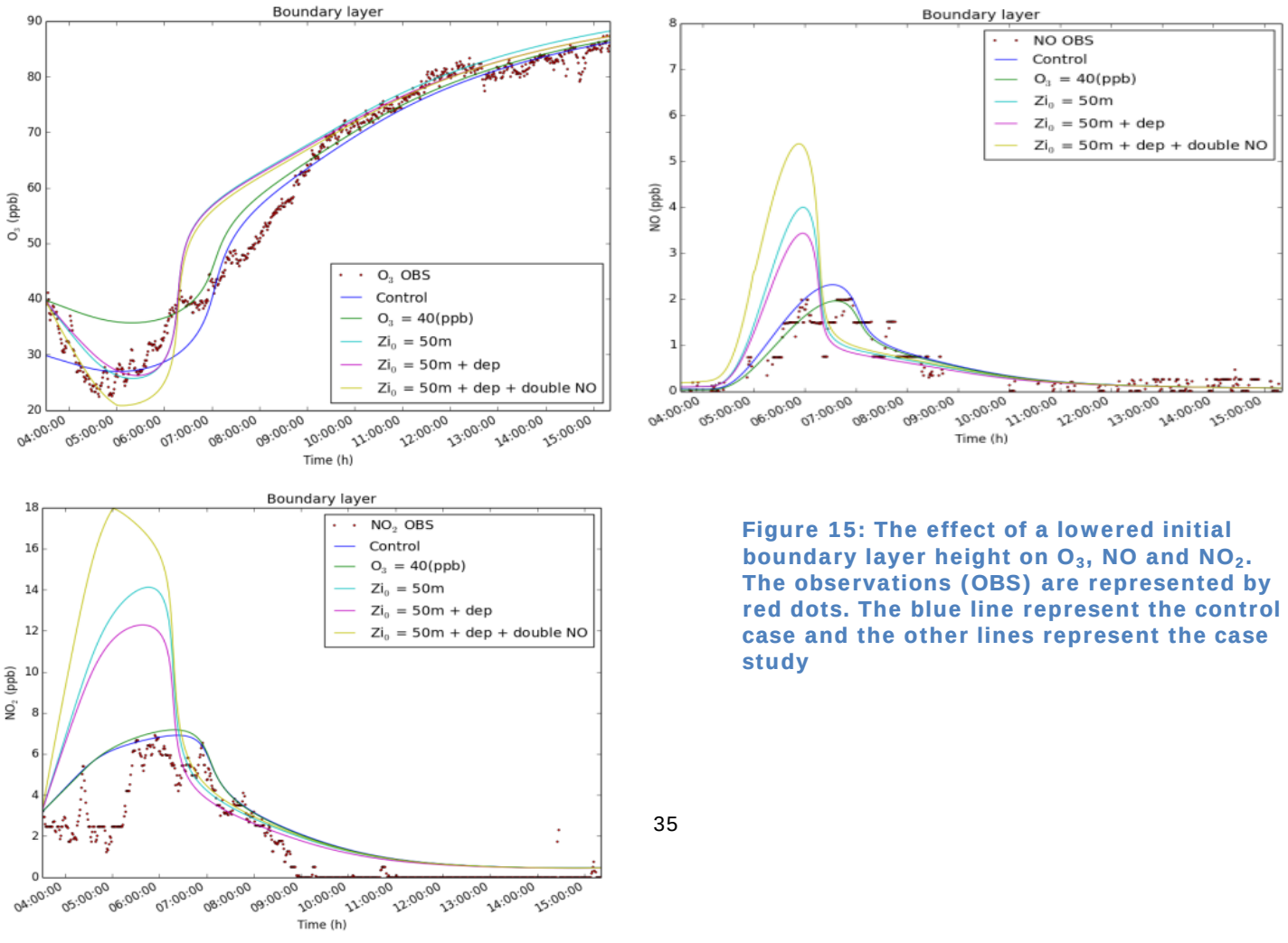

Figure 15: The effect of a lowered initial boundary layer height on O_3, NO and NO_2. The observations (OBS) are represented by red dots. The blue line represent the control case and the other lines represent the case study

4.2 Surface vs upper air conditions

Case 4: Lapse rates

We have tested three different types of free tropospheric O_3 lapse rates. In figure (16) the results of these three different types of lapse rates are presented. We clearly see that when the lapse rate is zero, the O_3 concentrations are decreasing (Cyan line). When we combine both structures, we see a small decrease in the concentrations (Magenta and yellow lines). The consequence of having a lapse is that the mixed-layer concentrations will increase. The lapse rate increases in the first place the concentrations in the free troposphere. These enhanced concentrations in the free troposphere are then mixed into the mixed layer.

In figure (17) the three different types of vertical O_3 profiles are shown. We see that the combined structures are the closest to the observations and will be the most likely profile shape. If we have no lapse rate, the O_3 concentrations stay to low and when we have a fixed lapse rate the O_3 concentrations get to high. This is also as expected; the observations that are made with the Zeppelin already suggested that we need some kind of combined structure. The modelled profiles indicate that the free tropospheric O_3 concentrations are increasing in time, while the observations are suggesting they stay constant (figure (17)).

When we compare the four case studies with each other, we see that case study 1 and 4 have their main effect on the O_3 concentrations after 7:00 AM. In contrast, cases 2 and 3, which have their main effect before 7:00 AM. Furthermore, we see that deposition has the smallest effect on the diurnal evolution of the O_3 and the lapse rate has the largest effect.

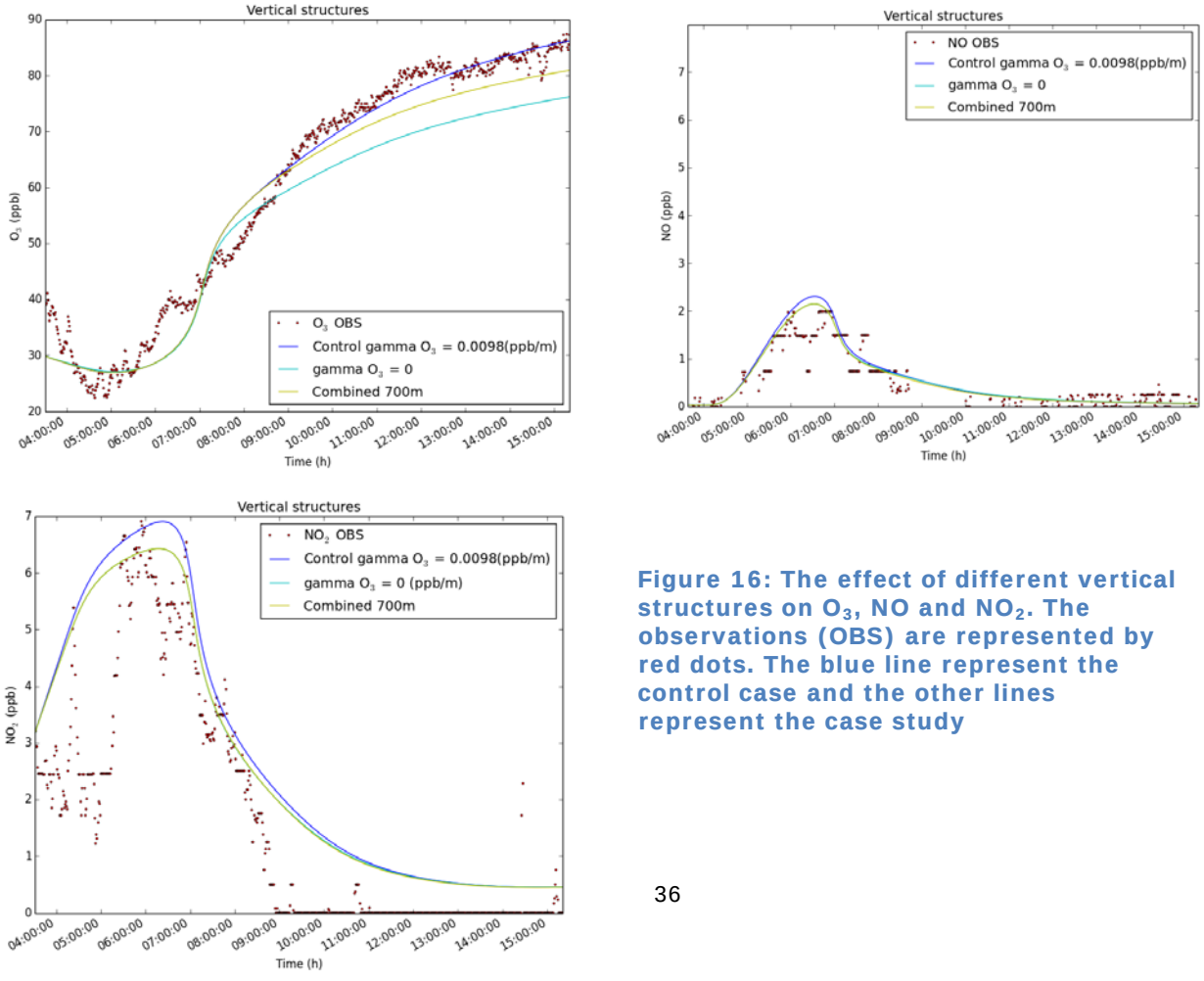

Figure 16: The effect of different vertical structures on O_3, NO and NO_2. The observations (OBS) are represented by red dots. The blue line represent the control case and the other lines represent the case study

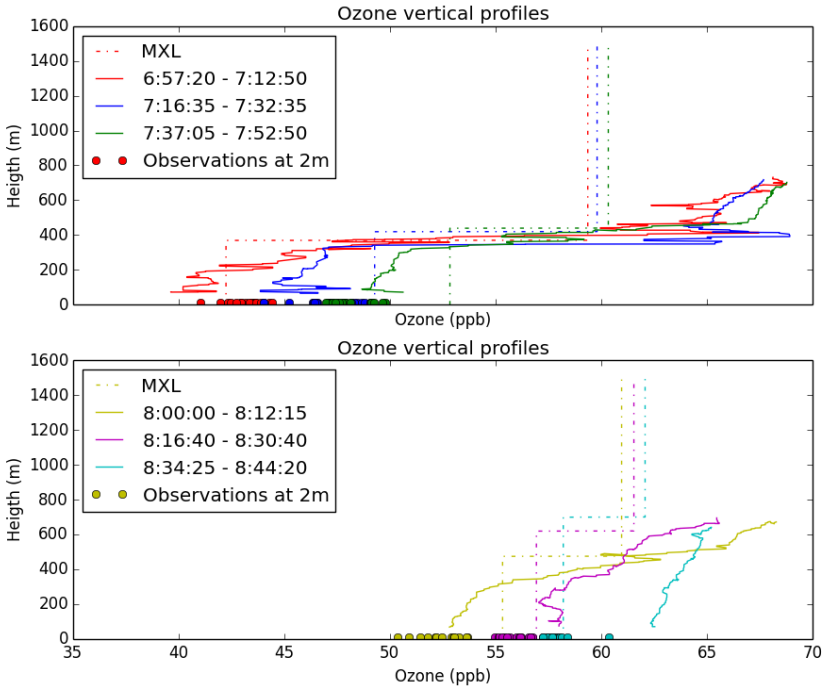

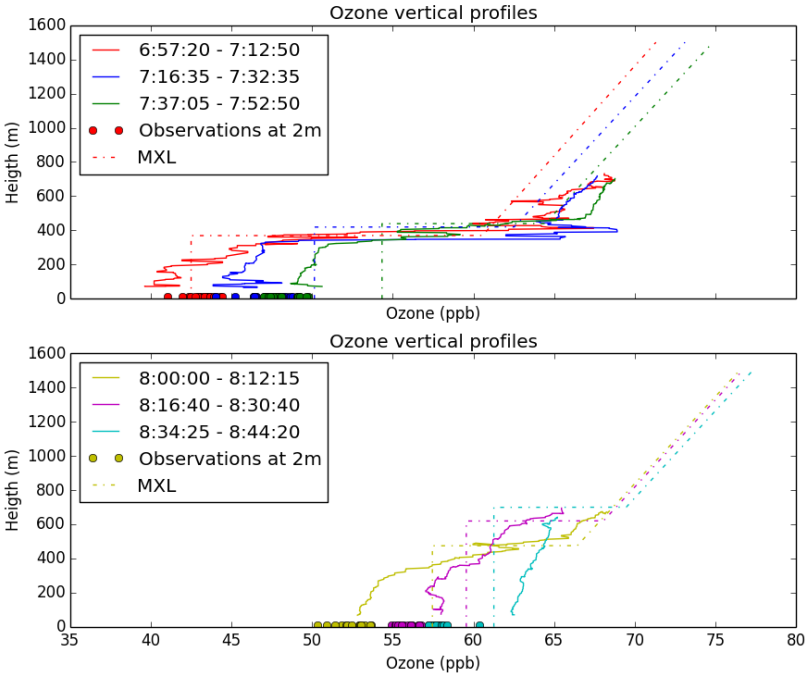

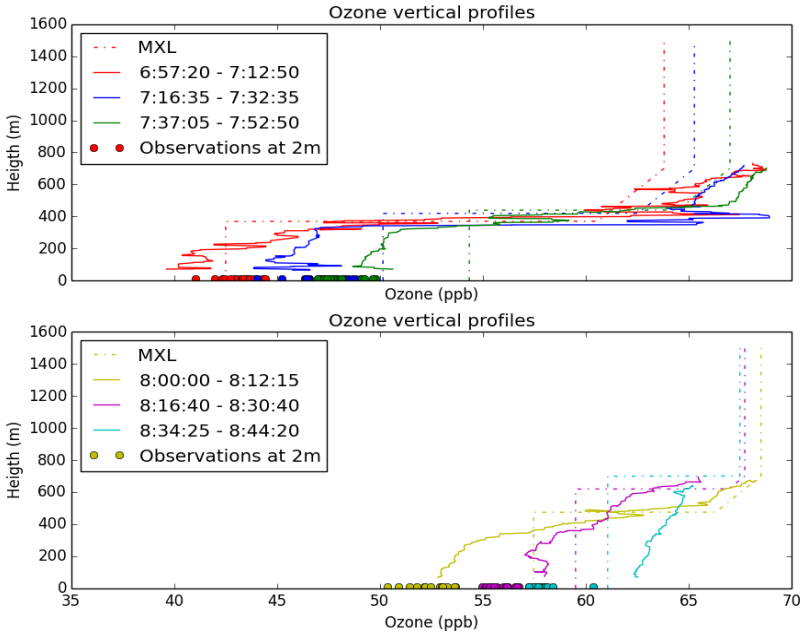

Figure 17: Three different vertical O_3 profiles. The solid lines represent the zeppelin observations, the dashed line the model output and the dots represent the surface measurements. Top left represents the profile with a zero lapse rate, top right represents the profile with the fixed lapse rate(0.0098 ppb / m) and down left the combination of the other two profiles

Discussion

In the first part of this research, a strong validated control case was made, in which we tried to validate the dynamics as well as the chemistry. To do so we used a mixed-layer model in which we were able to reproduce the temporal evolution of the key dynamics and chemistry. We demonstrated that the model is able to reproduce both the dynamics and chemistry in a reasonable way. However, we have also seen that we have many opportunities to adapt the model towards the observations. Within the model we have certain amount of freedom to turn the model ''knobs'' in order to improve the model output. We used observations to prescribe the initial and boundary conditions to calculate the surface fluxes and the temporal evolutions of potential temperature, specific moisture, boundary layer growth and chemical species. The tuning of these ''knobs'' happens within certain physical, realistic boundaries. In order to keep the model results realistic, we used observations, literature and/or expert judgement to constrain and validate the model. Important surface observations needed to validate the model dynamics are: the radiation components, temperature and relative humidity, and for chemistry we validated NO, NO_2 and O_3 concentrations.

Unique in this study is, that beside surface observations also upper-air observations are used which were measured by a Zeppelin platform. These upper-air observations allowed us to have an insight in the vertical structure and free tropospheric lapse rate of several variables (e.g. potential temperature, specific moisture and ozone). In this way we were also able to constrain the model in the vertical direction.

However, there are several points of consideration. The most fundamental point of consideration is that the model is actually not designed to investigate early morning conditions. During the morning, we have a stable and not well-mixed layer and one of the fundamental assumptions in the model is that the atmospheric quantities need to be well mixed across the whole CBL. Despite this problem the model still can be used as a first order guess. Such that we still can investigate the morning conditions and the morning O_3 decrease. The aim of the study was not to obtain the best fit with the observations, but to see the sensitivity of the system towards certain perturbations. Furthermore, we need to consider that some of the prescribed initial and boundary conditions in the control case are estimated values, based on literature and/or expert judgement. These values are not case specific and do possibly not apply for the case in San Pietro Capofiume. To improve the initial conditions used in the model, we need to improve the quantity and quality of the measurements. We still have a lack of data on the emission and deposition fluxes of O_3, NO and NO_2. Furthermore, we miss data on the initial concentrations, emission and deposition of VOC's and other compounds. This makes it very difficult to validate the chemistry correctly. In future research, I suggest to validate these compounds (OH, HO_2, ISOP) as well, to create a stronger validated control case. To do this more data from the Zeppelin platform could be used. Other processes that should be better quantified are advection and subsidence. They play a very important role in the diurnal evolution of the dynamics and chemistry. In the

model we also estimated the advection and subsidence within certain boundaries. When these processes are better constrained, the model can be better validated. It is also recommended to use an optimization formula in which we optimize all the initial settings and boundary conditions for all important parameters used in the model. Keeping in mind that these parameters need to be constrained within physically realistic values. Important parameters that should be considered are the emission fluxes for NO and NO_2, the free tropospheric lapse rates of O_3 and potential temperature, soil moisture and temperature and the advection of O_3 and heat.

In the second part of the research, we examined three case studies that possibly explain why the ozone concentrations in the morning are first decreasing. In the first case study we investigated the effect of dry deposition by plants on O_3 and NO_2 concentrations. Compared to the control case this case study was not very effective in improving the model. There was only a minor O_3 decrease visible in the afternoon (figure(13)). This minor effect was what we expected, since the stomata are not opened in the morning, resulting in a large stomatal resistance and thus a low deposition flux.

In the second case study, we investigated the effect of non-constant NO emissions. We emitted extra NO emissions at different times and intensity to mimic the effect of morning rush hour and emissions from agricultural land and industry. We have the highest observed NO concentrations between 7:00 and 8:00 AM, corresponding with the rush hour (figure(12)). Due to these high NO concentrations and low availability of light in the morning, O_3 will react with NO to produce NO_2. In this way the O_3 concentrations will be reduced in the morning. However, we see that we have the largest O_3 decrease when we emit NO before the rush hours starts (figure (14)). Meaning, that rush hour is likely not the main reason why O_3 concentrations are decreasing in the early morning. There are also other NO emitting sources in the morning that can contribute to the morning O_3 decrease. Possible sources that can emit NO are fertilized agricultural lands or industry nearby.

In the third case study we investigated the effect of a lowered initial boundary layer height. We expected when the initial boundary layer height is lowered the morning O_3 concentrations will decrease, due to a smaller volume and higher concentrated NO. In figure 15 we see that O_3 decreases sharply when the initial boundary layer height is lowered. Furthermore, when all three case studies are combined we see the total effect on the diurnal evolution of O_3. So, we showed that the calculated ozone decline is highly sensitive to the initial boundary layer height. Remember, that the MXL model is not suitable for describing stratified boundary layers, however it gives us a good first guess.

We need to keep in mind there are still other possibilities that can explain the morning O_3 decrease. For example, we did not investigate the role of VOC's on the diurnal evolution of O_3. It is expected that VOC's also play a large role in the production and destruction of O_3. Notice that the NO and NO_2 concentrations are increasing dramatically in the early morning, due to the combination of emissions and a shallow boundary layer. Our base simulation reproduces the observations adequately. This does not mean that our results are not correct, since we played with the ''knobs'' of the model and the fact that we estimated the emission

fluxes for both NO and NO_2. However, we kept the emissions within a realistic fixed fraction of each other, in which we have a three times higher emission for NO.

In the additional fourth case study we investigated three different vertical O_3 profiles. The main difference between them is that they all have a different free tropospheric O_3 lapse rate. In the first profile we used a free tropospheric O_3 lapse rate of zero, in the second profile we used a fixed lapse rate (0.0098 ppb/m) and in third profile we made a combination of the two profiles (figure (10)). We based these free tropospheric lapse rates and structures on the Zeppelin observations (appendix V figure (19)). When we compare the model output with the Zeppelin observations we see that the combined profile matches the best with the observations. However, when we have a look at the temporal evolution of the O_3 concentrations in figure (16), we see that the fixed lapse rate gives the best result compared to the surface observations. In this respect it is not clear which vertical O_3 profile is the best. Furthermore, we see that all modelled profiles indicate that the free tropospheric O_3 concentrations are increasing in time, while the observations are suggesting they stay constant (figure (17)). This indicates again the difficulties for the model to fit with the observations and stretches the importance of good qualitative and quantitative measurements on which the initial settings can be based.

When we compare the four case studies, we see that both the surface and upper-air conditions have a large impact on the diurnal evolution of O_3. We have seen that the surface conditions (NO emissions and initial boundary layer height) have their main impact on O_3 in the morning period and upper-air conditions (lapse rate) more in the afternoon. To be able to understand these early morning processes (stable and not well-mixed layer) it is advisable to use a model that resolved the vertical structure (e.g. a 1D model). Since the mixed-layer model used in this thesis is not designed for this purpose. However, as mentioned before the model is very suitable as a first characterization of the CBL dynamics and chemistry and to investigate the relative roles of chemistry and dynamics.

Conclusion

In this research, we investigated the early morning ozone decline in San Pietro Capofiume on the 12th of July. Our main findings are:

- The mixed-layer model is able to characterize the dynamics and chemistry very well
- Dry deposition by plants has the smallest effect on the diurnal evolution of O_3.
- The initial boundary layer height has the largest effect on the diurnal evolution of O_3.
- Surface conditions have more influence on the morning O_3 concentrations.
- Upper air conditions have more influence on the afternoon O_3 concentrations.
- A combination of two different free tropospheric lapse rates are the most promising in reconstructing the vertical O_3 profiles

References

Ainsworth, E. A., Yendrek, C. R., Sitch, S., Collins, W. J., & Emberson, L. D. (2012). The Effects of Tropospheric Ozone on Net Primary Productivity and Implications for Climate Change*. *Annual review of plant biology, 63*, 637-661.

Athanassiadis, G. A., Rao, S. T., Ku, J.-Y., & Clark, R. D. (2002). Boundary layer evolution and its influence on ground-level ozone concentrations. *Environmental Fluid Mechanics, 2*(4), 339-357.

Bonafe, G. (Ed.). (2009). *SRNWP data pool: the meteorological site of San Pietro Capofiume, Italy*. Bologna: ARPA-SIMC Servizio Idro-Meteo-Clima.

Bouwman, A., Boumans, L., & Batjes, N. (2002). Modeling global annual N2O and NO emissions from fertilized fields. *Global Biogeochemical Cycles, 16*(4), 28-21-28-29.

Burns, S., Horst, T., Jacobsen, L., Blanken, P., & Monson, R. (2012). Using sonic anemometer temperature to measure sensible heat flux in strong winds. *Atmospheric Measurement Techniques, 5*(9), 2095-2111.

Conzemius, R. J., & Fedorovich, E. (2006). Dynamics of sheared convective boundary layer entrainment. Part I: Methodological background and large-eddy simulations. *Journal of the atmospheric sciences, 63*(4), 1151-1178.

Ganzeveld, L., Eerdekens, G., Feig, G., Fischer, H., Harder, H., Königstedt, R., . . . Scheeren, H. (2008). Surface and boundary layer exchanges of volatile organic compounds, nitrogen oxides and ozone during the GABRIEL campaign. *Atmospheric Chemistry and Physics, 8*(20), 6223-6243.

Horii, C. V., Munger, J. W., Wofsy, S. C., Zahniser, M., Nelson, D., & McManus, J. B. (2004). Fluxes of nitrogen oxides over a temperate deciduous forest. *Journal of Geophysical Research: Atmospheres (1984–2012), 109*(D8).

Jacob, D. (1999). *Introduction to atmospheric chemistry*: Princeton University Press.

Jacob, D. J. (2000). Heterogeneous chemistry and tropospheric ozone. *Atmospheric Environment, 34*(12), 2131-2159.

Jana, P., Sarkar, D., Saha, D., & Midya, S. (2012). Effect of cloud occurrences on tropospheric ozone over, Alipore (22.52° N, 88.33° E), India. *Journal of earth system science, 121*(3), 711-722.

Morris, G. A., Ford, B., Rappenglück, B., Thompson, A. M., Mefferd, A., Ngan, F., & Lefer, B. (2010). An evaluation of the interaction of morning residual layer and afternoon mixed layer ozone in Houston using ozonesonde data. *Atmospheric Environment, 44*(33), 4024-4034.

Neu, U., Künzle, T., & Wanner, H. (1994). On the relation between ozone storage in the residual layer and daily variation in near-surface ozone concentration—A case study. *Boundary-Layer Meteorology, 69*(3), 221-247.

Ouwersloot, H., Vilà-Guerau de Arellano, J., Nölscher, A., Krol, M., Ganzeveld, L., Breitenberger, C., . . . Lelieveld, J. (2012). Characterization of a boreal convective boundary layer and its impact on atmospheric chemistry during HUMPPA-COPEC-2010. *Atmospheric Chemistry and Physics, 12*(19), 9335-9353.

Parrish, D., Trainer, M., Williams, E., Fahey, D., Hübler, G., Eubank, C., . . . Fehsenfeld, F. (1986). Measurements of the NO x - O3 photostationary state at Niwot Ridge, Colorado. *Journal of Geophysical Research: Atmospheres (1984–2012), 91*(D5), 5361-5370.

Pino, D., Vilà-Guerau de Arellano, J., & Duynkerke, P. G. (2003). The contribution of shear to the evolution of a convective boundary layer. *Journal of the atmospheric sciences, 60*(16), 1913-1926.

Rohrer, F. (2012). *PEGASOS 2012 : NOx, CO, O3*. Power Point Bologna.

Schüttemeyer, D., Moene, A., Holtslag, A., & De Bruin, H. (2008). Evaluation of Two Land Surface Schemes Used in Terrains of Increasing Aridity in West Africa. *Journal of Hydrometeorology, 9*(2).

Stevenson, D., Dentener, F., Schultz, M., Ellingsen, K., Van Noije, T., Wild, O., . . . Bell, N. (2006). Multimodel ensemble simulations of present - day and near - future tropospheric ozone. *Journal of Geophysical Research: Atmospheres (1984 - 2012), 111*(D8).

Stull, R. (1988). *An introduction to boundary layer meteorology* (first edition ed.). Madison: Kluwer Academic.

Super, I. (2013). *The interaction between air quality and climate change and their potential for environmental conflicts.* (Master), Wageningen University, Wageningen.

Vilà Guerau de Arellano, J., Patton, E. G., Karl, T., van den Dries, K., Barth, M. C., & Orlando, J. J. (2011). The role of boundary layer dynamics on the diurnal evolution of isoprene and the hydroxyl radical over tropical forests. *Journal of Geophysical Research: Atmospheres (1984–2012), 116*(D7).

vilà Guerau de Arellano, J., & van Heerwaarden, C. (2013). *Atmospheric boundary layer: Integrating air chemistry and land interactions*. Wageningen.

Zhang, J., & Rao, S. T. (1999). The role of vertical mixing in the temporal evolution of ground-level ozone concentrations. *Journal of Applied Meteorology, 38*(12), 1674-1691.

Appendix I: Measurement stations with their measured variables

Table 2: Types of Measurement stations with their variables

Surface meteorological station:		
Instrument	**Variable**	**Time res.**
Cup anemometer (Vaisala QMW110)	Wind speed (m/s)	1h
	Wind direction (degrees)	1h
Radiometer (Kipp & Zonen CNR1)	Downward short-wave radiation (Wm2)	1h
	Upward short-wave radiation (Wm2)	1h
	Downward long-wave radiation (Wm2)	1h
	Upward long-wave radiation (Wm2)	1h
Thermohygrometer (Vaisala QMH102)	Temperature (K)	1h
	Relative humidity (%)	1h
Barometer (Vaisala PMT16A)	Atmospheric pressure (hPa)	1h
Rain gauge (Vaisala QMR102)	Precipitation rate (mm/h)	1h
Leaf wetness sensor (Vaisala QLW101)	Leaf wetness (minutes)	1h

Ground Station:		
Instrument	**Variable**	**Time res.**
Time-Domain Reflectometer	Soil water content(m3/m3)	1h
Resistive thermometers	Soil temperature (m3/m3)	1h

Radio sonde Station:		
Instrument	**Variable**	**Time res.**
Radio sonde (Vaisala RS92)	Temperature (K)	6h to 24h
	Relative humidity (%)	6h to 24h
	Wind speed (m/s) 6	6h to 24h
	Wind direction (degrees)	6h to 24h
	Virtual potential temperature (K)	6h to 24h

Ground based remote sensing station:		
Instrument	**Variable**	**Time res.**
LiDAR-ceilometer (Vaisala LD-40)	Range corrected signal (dB)	15m

Air quality station:		
Instrument	**Variable**	**Time res.**
Air quality station	Nitrogen dioxide mass concentration (gm3)	1h
	Ozone mass concentration (gm3)	1h
	PM10 mass concentration (gm3)	24h
Micrometeorological station:		

Instrument	Variable	Time res.
Sonic anemometer (Metek USA-1 Research)	Wind speed (m/s)	30m
	Wind direction (degrees)	30m
	Sonic temperature (K)	30m
	St. dev. of wind direction (m/s)	30m
	St.dev. of the 3 wind components (m/s)	30m
	Turbulent kinetic energy (m2/s2)	30m
	St.dev. of temperature (K)	30m
	Covariances between wind components(-)	30m
	Covariances between wind components and temperature (-)	30m
	Friction velocity (ms⁻1)	30m
	Ratio between anemometer height and Monin-Obukhov length	30m
	Scale temperature (K)	30m
	Uncorrected turbulent heat flux (Wm2)	30m
	Structure parameters of u,v,w,T	30m
Infrared Gas Analyzer (LiCor LI-7500)	Water vapor mass concentration gm3	30m
	Carbon dioxide mass concentration(gm3)	30m
	St.dev. of water vapor mass concentration (mgm3)	30m
	St.dev. of carbon dioxide mass concentration (mgm3)	30m
Sonic anemometer + Infrared Gas Analyzer	Vertical flux of water vapor gm2 s	30m
	Vertical ux of carbon dioxide (gm2 s)	30m
	Turbulent latent heat flux (Wm2)	30m
	Corrected turbulent sensible heat flux (Wm2)	30m
Radiometer (Kipp & Zonen CNR1)	Downward short-wave radiation (Wm2)	1h
	Upward short-wave radiation (Wm2)	1h
	Downward long-wave radiation (Wm2)	1h
	Upward long-wave radiation (Wm2)	1h
	Net radiation (Wm2)	1h
	Sky temperature (K)	1h
	Ground temperature (K)	1h
	Albedo (-)	1h
Ground heat flux plate (Hukseflux)	Heat flux into the ground at 5cm depth(Wm2)	1h

Appendix II: Chemical reaction scheme used in the MXLCH model.

Table 2: Reaction scheme used in the MXLCH model. (Ouwersloot et al., 2012).

Name	Chemical equation	Reaction rate constant
R1	$O_3 + h\nu \rightarrow O^{1D} + O_2$	$3.83\times10^{-5} \cdot e^{-\frac{0.575}{\cos(\chi)}}$
R2	$O^{1D} + H_2O \rightarrow 2\,OH$	$1.63\times10^{-10} \cdot e^{\frac{60}{T}}$
R3	$O^{1D} + N_2 \rightarrow O_3 + REST$	$2.15\times10^{-11} \cdot e^{\frac{110}{T}}$
R4	$O^{1D} + O_2 \rightarrow O_3$	$3.30\times10^{-11} \cdot e^{\frac{55}{T}}$
R5	$NO_2 + h\nu \rightarrow NO + O_3 + REST$	$1.67\times10^{-2} \cdot e^{-\frac{0.575}{\cos(\chi)}}$
R6	$CH_2O + h\nu \rightarrow HO_2 + REST$	$1.47\times10^{-4} \cdot e^{-\frac{0.575}{\cos(\chi)}}$
R7	$OH + CO \rightarrow HO_2 + CO_2 + REST$	2.40×10^{-13}
R8	$OH + CH_4 \rightarrow CH_3O_2 + REST$	$2.45\times10^{-12} \cdot e^{\frac{-1775}{T}}$
R9	$OH + C_5H_8 \rightarrow RO_2$	1.00×10^{-10}
R10	$OH + MVK \rightarrow HO_2 + CH_2O + REST$	2.40×10^{-11}
R11	$HO_2 + NO \rightarrow OH + NO_2$	$3.50\times10^{-12} \cdot e^{\frac{250}{T}}$
R12	$CH_3O_2 + NO \rightarrow HO_2 + NO_2 + CH_2O + REST$	$2.80\times10^{-12} \cdot e^{\frac{300}{T}}$
R13	$RO_2 + NO \rightarrow HO_2 + NO_2 + CH_2O + MVK$	1.00×10^{-11}
R14	$OH + CH_2O \rightarrow HO_2 + REST$	$5.50\times10^{-12} \cdot e^{\frac{125}{T}}$
R15	$2\,HO_2 \rightarrow H_2O_2 + O_2$	k^1
R16	$CH_3O_2 + HO_2 \rightarrow REST$	$4.10\times10^{-13} \cdot e^{\frac{750}{T}}$
R17	$RO_2 + HO_2 \rightarrow REST$	1.50×10^{-11}
R18	$OH + NO_2 \rightarrow HNO_3$	$3.50\times10^{-12} \cdot e^{\frac{340}{T}}$
R19	$NO + O_3 \rightarrow NO_2 + O_2$	$3.00\times10^{-12} \cdot e^{-\frac{1500}{T}}$
R20	$OH + HO_2 \rightarrow H_2O + O_2$	$4.80\times10^{-11} \cdot e^{\frac{250}{T}}$
R21	$OH + H_2O_2 \rightarrow H_2O + HO_2$	$2.90\times10^{-12} \cdot e^{\frac{-160}{T}}$
R22	$NO + NO_3 \rightarrow 2\,NO_2$	$1.80\times10^{-11} \cdot e^{\frac{110}{T}}$
R23	$NO_2 + O_3 \rightarrow NO_3 + O_2$	$1.40\times10^{-13} \cdot e^{\frac{-2470}{T}}$
R24	$NO_2 + NO_3 \rightarrow N_2O_5$	k^2
R25	$N_2O_5 \rightarrow NO_2 + NO_3$	k^3
R26	$N_2O_5 + H_2O \rightarrow 2\,HNO_3$	2.50×10^{-22}
R27	$N_2O_5 + 2\,H_2O \rightarrow 2\,HNO_3 + H_2O$	1.80×10^{-39}

Appendix III: Initial boundary layer condition dynamics and chemistry

Table 3: Initial boundary layer conditions atmosphere used in the MXLCH model.

Variable	Description and unit	Value
latt	latitude (º)	44.654
long	longitude (º)	11.623
doy	Day of the year	193
zi0	Inital boundary layer heigth (m)	150
β	entrainment ratio (-)	0.2
wsls	Flow divergence factor for subsidence (s^{-1})	1.00E-06
γ	Potential temprature lapse rate in FT (Km^{-1})	0.0046
θm0	Initial mixed layer potential temprature (K)	293.5
dθ0	Initial potential temperature jump (K)	4.4
advθ	Advection of potential temperature (Ks^{-1})	0.000145
pressure	Air pressure in the boundary layer (Pa)	1010
γq	Specific humidity lapse rate in the free troposphere (gkg^{-1} m^{-1})	-0.0014
qm0	Initial mixed layer specific humidity (gkg^{-1})	11
dq0	Initial specific humidity jump (gkg^{-1})	-0.8
advq	Advection of specific humidity ($gkg^{-1}s^{-1}$)	0
z0	Roughness length (m)	0.02
um0	Initial u in mixed layer (ms^{-1})	6
vm0	Initial v in mixed layer (ms^{-1})	-4
ug	Geostrophic wind in the x-direction (ms^{-1})	10
vg	Geostrophic wind in the y-direction (ms^{-1})	0
z0m	Roughness length for momentum (m)	0.02
z0h	Roughness length for heat (m)	0.002
cc	Cloud cover (-)	0.01
S0	Incoming shortwave radiation (Wm^{-2})	1368
albedo	Albedo (-)	0.17

Table 4: Initial boundary layer conditions surface used in the MXLCH model

Variable	Description and unit	Value
Ts	initial surface temperature (K)	300
w2	volumetric water content deeper soil layer (m3 m-3)	0.219
wg	volumetric water content top soil layer (m3 m-3)	0.14
wwilt	volumetric water content wilting point (m3 m-3)	0.171
wfc	volumetric water content field capacity (m3 m-3)	0.323
wsat	saturated volumetric water content (m3 m-3)	0.472
Tsoil	temperature top soil layer (K)	294
T2	temperature deeper soil layer (K)	284

Table 5: Initial boundary layer conditions chemical species used in the MXLCH model.

Chemical Species	Initial mixed-layer mixing ratio (ppb)	Initial free troposphere mixing ratio (ppb)	Surface emission (ppb m/s)	Advection (ppb m/s)	Shape of the emission evolution
O3	30	58	0.025*	0.0003	5
NO	0.17	0.17	0.078	0	1
NO2	3	3	0.026	0	1
CH4	1724	1724	0	0	1
ISO	0	0	0.05	0	1
HO2	0	0	0	0	1
CO	140	140	0	0	0

Table 6: Explanation of the shape of the emission.

0	No emission at all
1	A constant emission
2	An emission that evolves in time as a sinusoid. In between the emission is a sinusoid who's phase ranges from 0 to π . The maximum value of the sinusoid is given by the emission value listed in table 3.
3	An emission that is constant during daytime. In between the emission is constantly equal to the emission value listed in table 3
4	An emission that evolves in time as a cosine. In between the emission behaves like a flipped cosine (a cosine who's phase ranges from $-\pi$ to π) with a mean and an amplitude which are both equal to half the emission value listed in table 3.
5	Dry deposition of atmospheric compounds according to $-vc\ C$. The deposition velocity vc in m s^{-1} needs to be specified. The velocity is equal to the emission listed in table 3.
6	Dry deposition via plants. The deposition velocity is dynamically calculated.

Appendix IV: Vertical profiles for potential temperature and specific moisture.

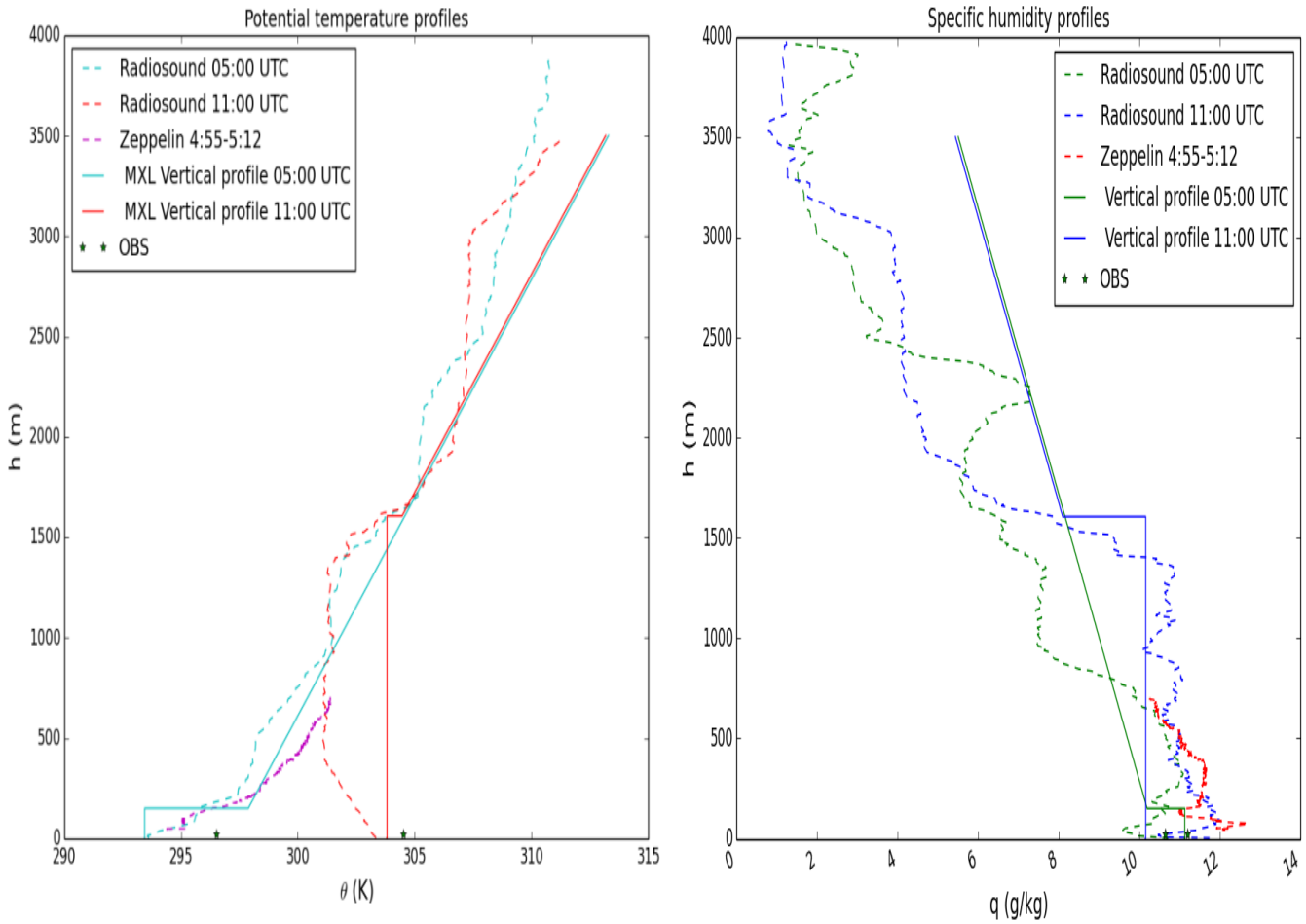

Figure 18: Evolution of the vertical profiles of the potential temperature (left) and specific moisture (right) measured by radio sondes on 12 July 2012 (05:00 and 11:00 UTC). In both profiles the striped lines represent the observations from the radio sondes and the zeppelin(magenta and red). The solid lines represent a reconstruction of the vertical profiles, from the model.

Appendix V: Vertical profiles O_3

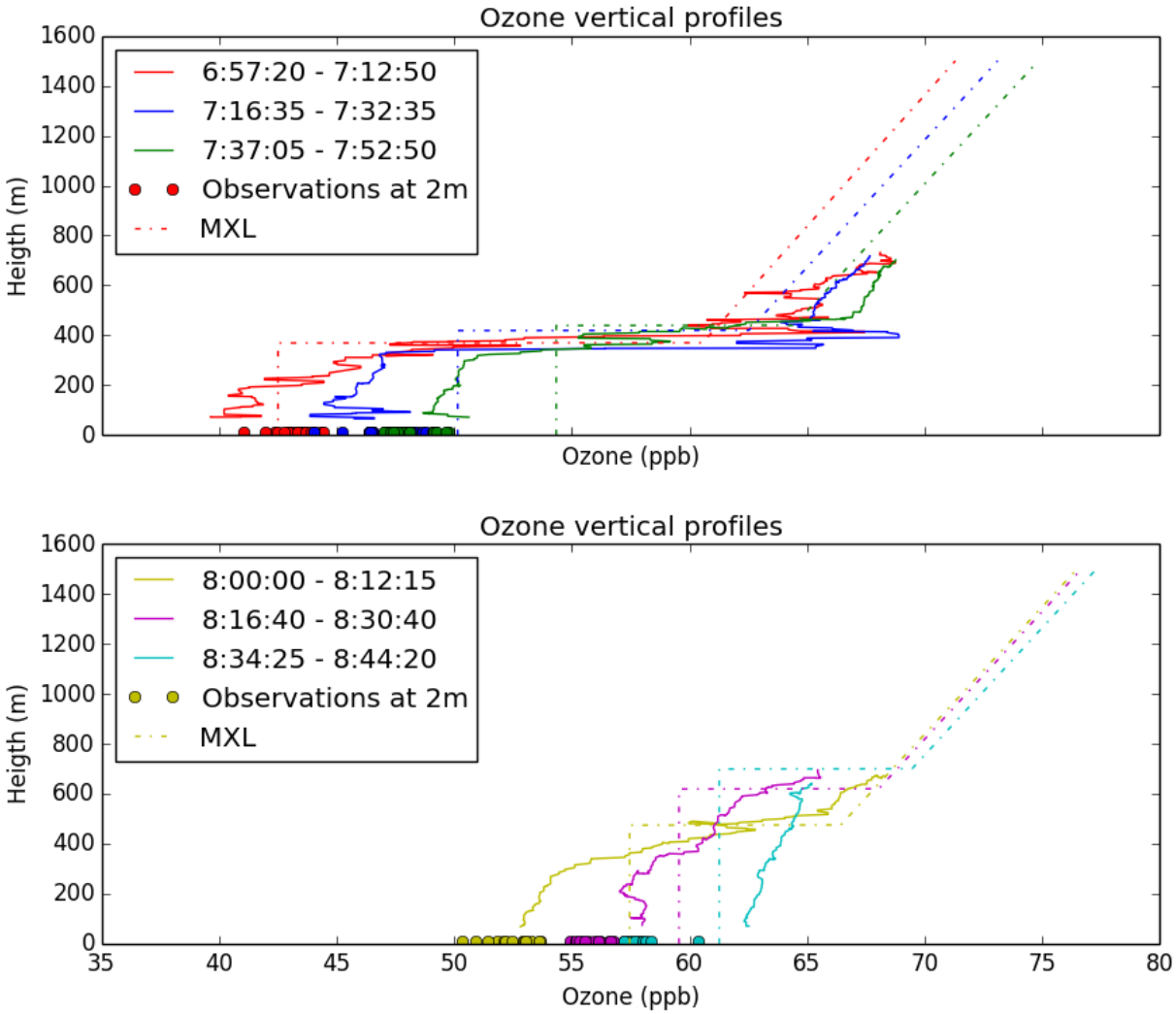

Figure 19: Vertical profile for ozone at different times during the day. Solid lines represent zeppelin data, dashed lines the model output and the dots are the surface observations

Appendix VI: Specifications for the case studies

Table 7: Case 1, Dry deposition of O_3 and NO_2 by plants

	Name run	Control	Deposition O3	Deposition NO2	Deposition O3 + NO2
O3	Initial mixed layer concentration	30	30	30	30
	Initial free troposphere concentration	58	58	58	58
	Advection	0.0003	0.0003	0.0003	0.0003
	free tropospheric lapse rate	0.0098	0.0098	0.0098	0.0098
	Constant deposition velocity	0.0025	**x**	0.0025	**x**
	Dynamical depostion velocity	x	**yes**	x	**yes**
NO	Initial mixed layer concentration	0.17	0.17	0.17	0.17
	Initial free troposphere concentration	0.17	0.17	0.17	0.17
	Initial emission	0.078	0.078	0.078	0.078
	Extra emission	0	0	0	0
	Emission time	0	0	0	0
NO2	Initial mixed layer concentration	3	3	3	3
	Initial free troposphere concentration	3	3	3	3
	Initial emission	0.026	0.026	0.026	0.026
	Dynamical depostion velocity	x	x	**yes**	**yes**
CBL	Initial boundary layer height	150	150	150	150

Table 8: Case 2, Non constant NO emissions

	Name run	Control	Double NO emissions (3:30-5:00)	Fourfold NO emissions (3:30-5:00)	Fourfold NO emissions (5:00-6:30)	Rush Hour (7:00-9:00)
O3	Initial mixed layer concentration	30	30	30	30	30
	Initial free troposphere concentration	58	58	58	58	58
	Advection	0.0003	0.0003	0.0003	0.0003	0.0003
	free tropospheric lapse rate	0.0098	0.0098	0.0098	0.0098	0.0098
	Constant deposition velocity	0.0025	**x**	**x**	**x**	**x**
	Dynamical depostion velocity	x	**yes**	**yes**	**yes**	**yes**
NO	Initial mixed layer concentration	0.17	0.17	0.17	0.17	0.17
	Initial free troposphere concentration	0.17	0.17	0.17	0.17	0.17
	Initial emission	0.078	0.078	0.078	0.078	0.078
	Extra emission	0	**0.156**	**0.312**	**0.312**	**0.312**
	Emission time	0	**3:30-5:00**	**3:30-5:00**	**5:00-6:30**	**7:00-9:00**
NO2	Initial mixed layer concentration	3	3	3	3	3
	Initial free troposphere concentration	3	3	3	3	3
	Initial emission	0.026	0.026	0.026	0.026	0.026
	Dynamical depostion velocity	x	**yes**	**yes**	**yes**	**yes**
CBL	Initial boundary layer height	150	150	150	150	150

Table 9: Case 3, boundary layer

	Name run	Control	O3 = 40ppb	Initial Boundary layer 50m	BLH + Dep	BLH+Dep+NO
O3	Initial mixed layer concentration	30	**40**	**40**	**40**	**40**
	Initial free troposphere concentration	58	58	58	58	58
	Advection	0.0003	0.0003	0.0003	0.0003	0.0003
	free tropospheric lapse rate	0.0098	0.0098	0.0098	0.0098	0.0098
	Constant deposition velocity	0.0025	0.0025	0.0025	**x**	**x**
	Dynamical depostion velocity	x	x	x	**yes**	**yes**
NO	Initial mixed layer concentration	0.17	0.17	0.17	0.17	0.17
	Initial free troposphere concentration	0.17	0.17	0.17	0.17	0.17
	Initial emission	0.078	0.078	0.078	0.078	0.078
	Extra emission	0	0	0	0	**0.156**
	Emission time	0	0	0	0	**3:30-5:00**
NO2	Initial mixed layer concentration	3	3	3	3	3
	Initial free troposphere concentration	3	3	3	3	3
	Initial emission	0.026	0.026	0.026	0.026	0.026
	Dynamical depostion velocity	x	x	x	**yes**	**yes**
CBL	Initial boundary layer height	150	150	**50**	**50**	**50**

Table 10: Case 4, different vertical stuctures

	Name run	Control	Gamma O3 = 0 (ppb/m)	Combined 1000m	combined 700m
O3	Initial mixed layer concentration	30	30	30	30
	Initial free troposphere concentration	58	58	58	58
	Advection	0.0003	0.0003	0.0003	0.0003
	free tropospheric lapse rate	0.0098	0	after 1000m= 0 (ppb/m)	after 700m = 0 (ppb/m)
	Constant deposition velocity	0.0025	0.0025	0.0025	0.0025
	Dynamical depostion velocity	x	x	x	x
NO	Initial mixed layer concentration	0.17	0.17	0.17	0.17
	Initial free troposphere concentration	0.17	0.17	0.17	0.17
	Initial emission	0.078	0.078	0.078	0.078
	Extra emission	0	0	0	0
	Emission time	0	0	0	0
NO2	Initial mixed layer concentration	3	3	3	3
	Initial free troposphere concentration	3	3	3	3
	Initial emission	0.026	0.026	0.026	0.026
	Dynamical depostion velocity	x	x	x	x
CBL	Initial boundary layer height	150	151	152	153